Mon. Mar. 19, 2018

- Exam and Semester Avg. Grades

- Radar (Ch. 6) Part 1

- Reading: Finish Ch. 6, Start Ch. 7 (Radar)

  Also: For lab on Wed., jump ahead and read part of Ch. 8 (pg. 281-287) on Multispectral Classification, especially Fig. 8-31 & 8-32.

Radar

- Broken up into Ch. 6 (theory) and Ch. 7 (applications)

- It will be on Final Exam but not on Midterm, since we won't have time for Radar homework

- Once again the radar INSTRUMENTS Sabins describes are old and obsolete, but the theory/techniques still apply

Midterm Exam Results

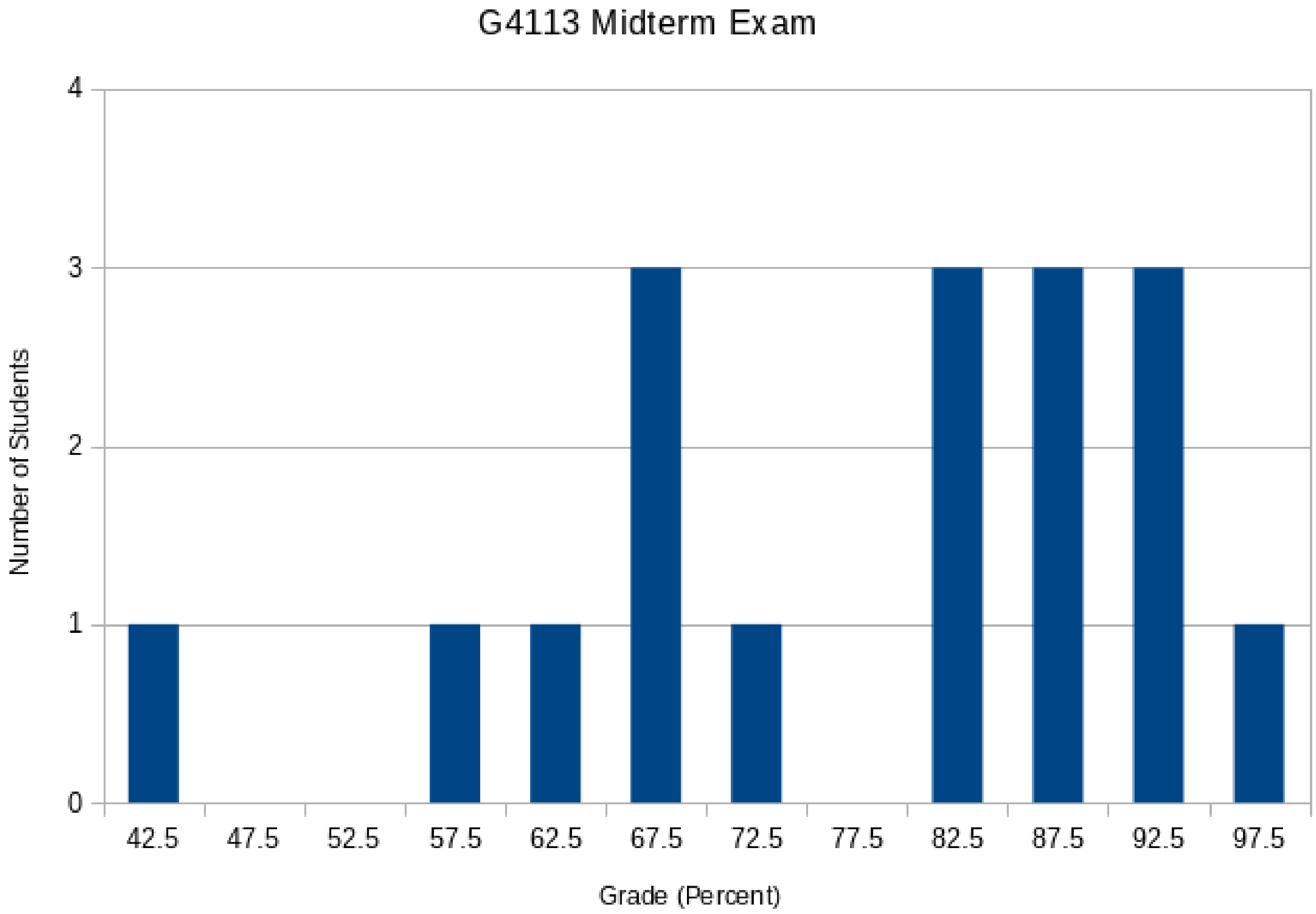

- Median 82, Average 77
- Review #4, #6, #9, and #11

Semester Averages

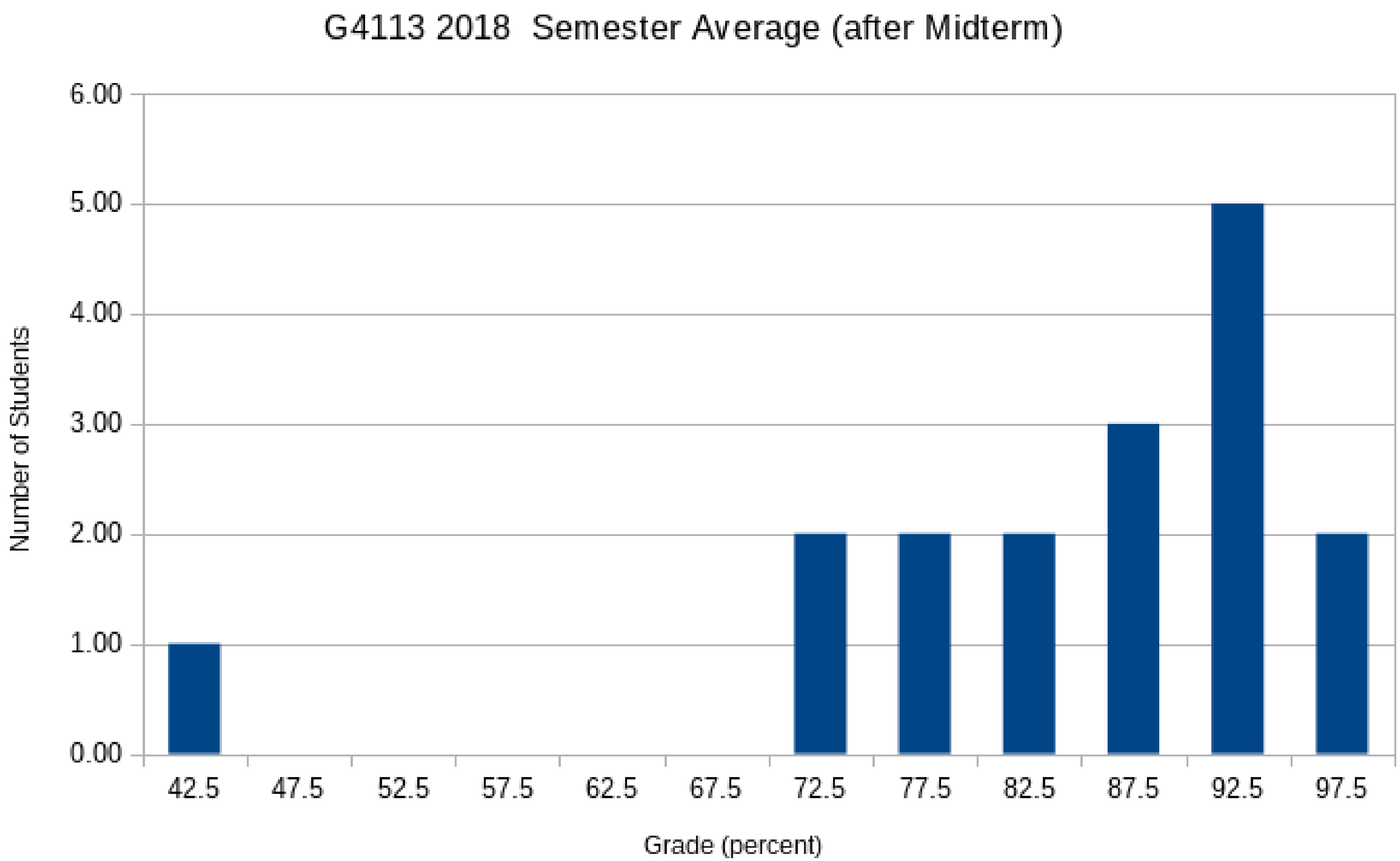

- End-of-semester averages will probably be slightly lower, since they will include final exam, and exam grades are on average a little lower than lab+homework.

Radar Advantages

- Penetrates clouds
  - Especially important for tropics and high latitudes (sea ice)
  - Venus, Titan, subsurface of Mars
- Penetrates to "moderate" depth in surface (varies with wavelength)
- Can obtain information on ~cm to ~m scale structure
  - Longer wavelength ~matches structure size
  - Can use polarization information
- Interferometry can measure ~cm scale motion
  - Motion on faults, subsidence, glaciers
- Can sense moisture content in soils

Radarsat-2: North end of Sermilik fjord, Greenland

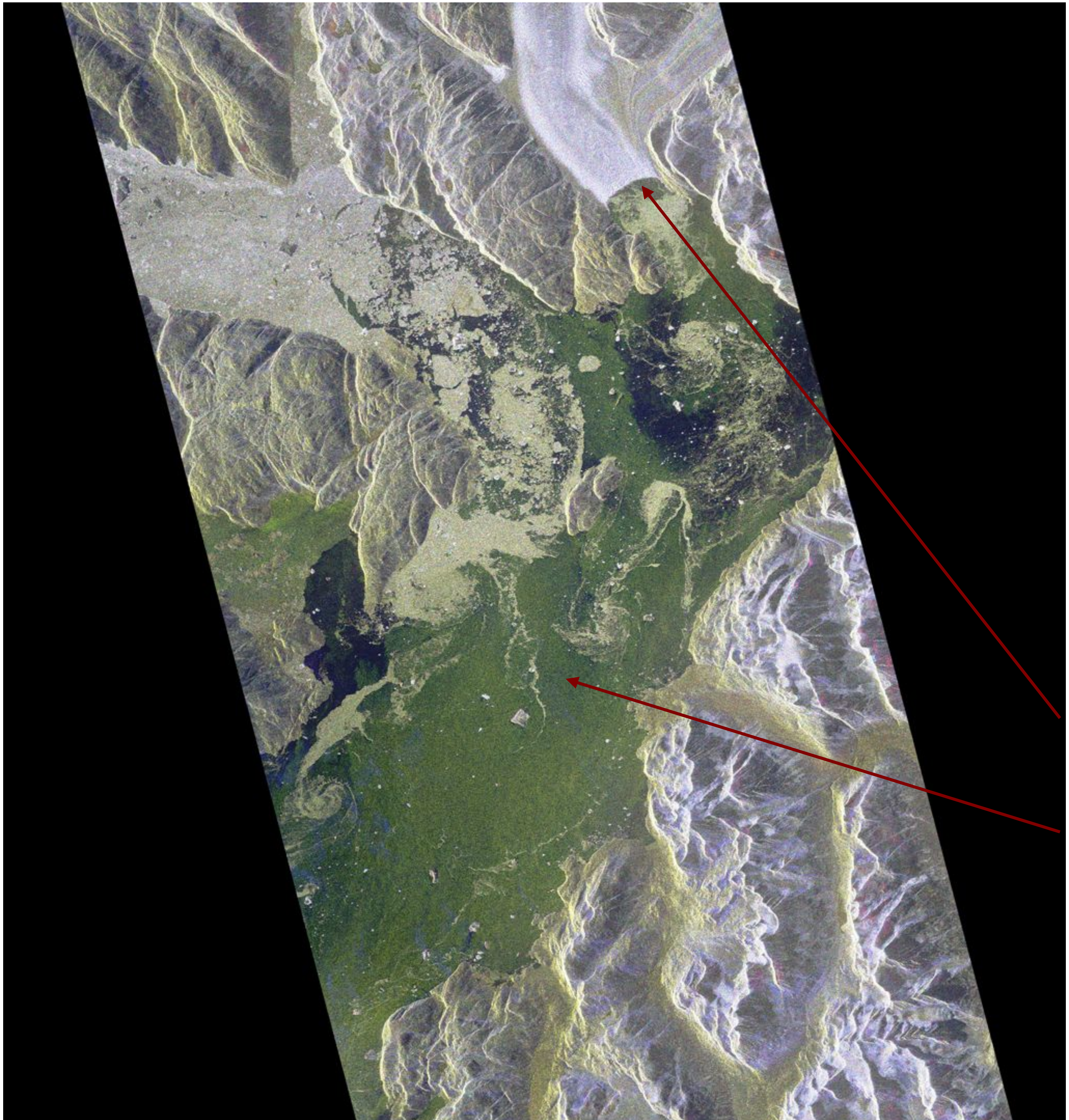

RGB = (HH, V V, HV)

25km x 50km

25m resolution

Fenrisgletscher glacier

Fjord, with different types of sea ice and leads (open water)

Radarsat-2: Iqaluit community Frobisher Bay, Baffin Island

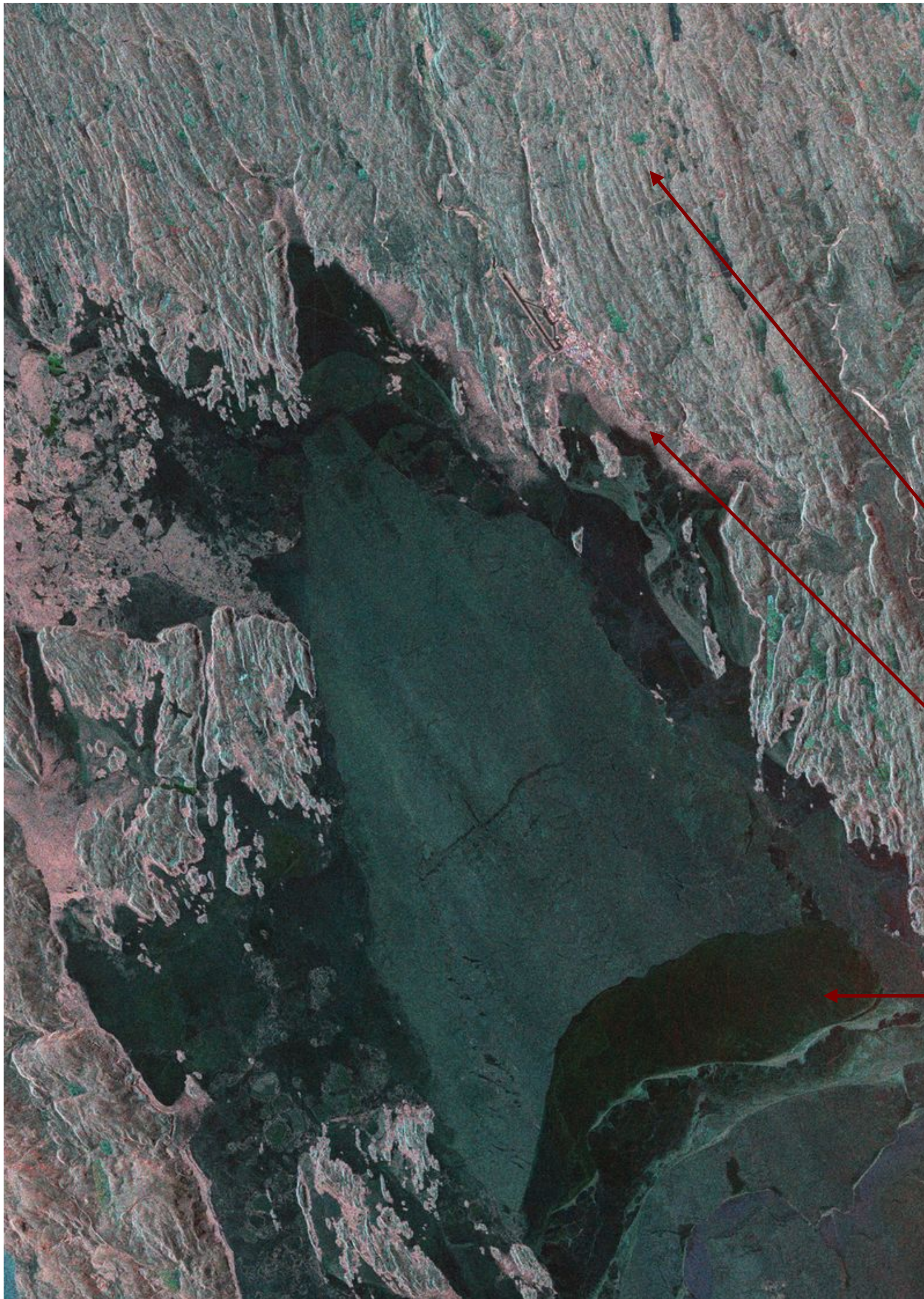

RGB = (HH, V V, HV)

25km x 28km

8m resolution

Striations,
typical of glaciated terrain

Community, Airfield

Bay mostly ice covered,
but large tidal variations
open up leads

Venus, Magellan Spacecraft: Craters

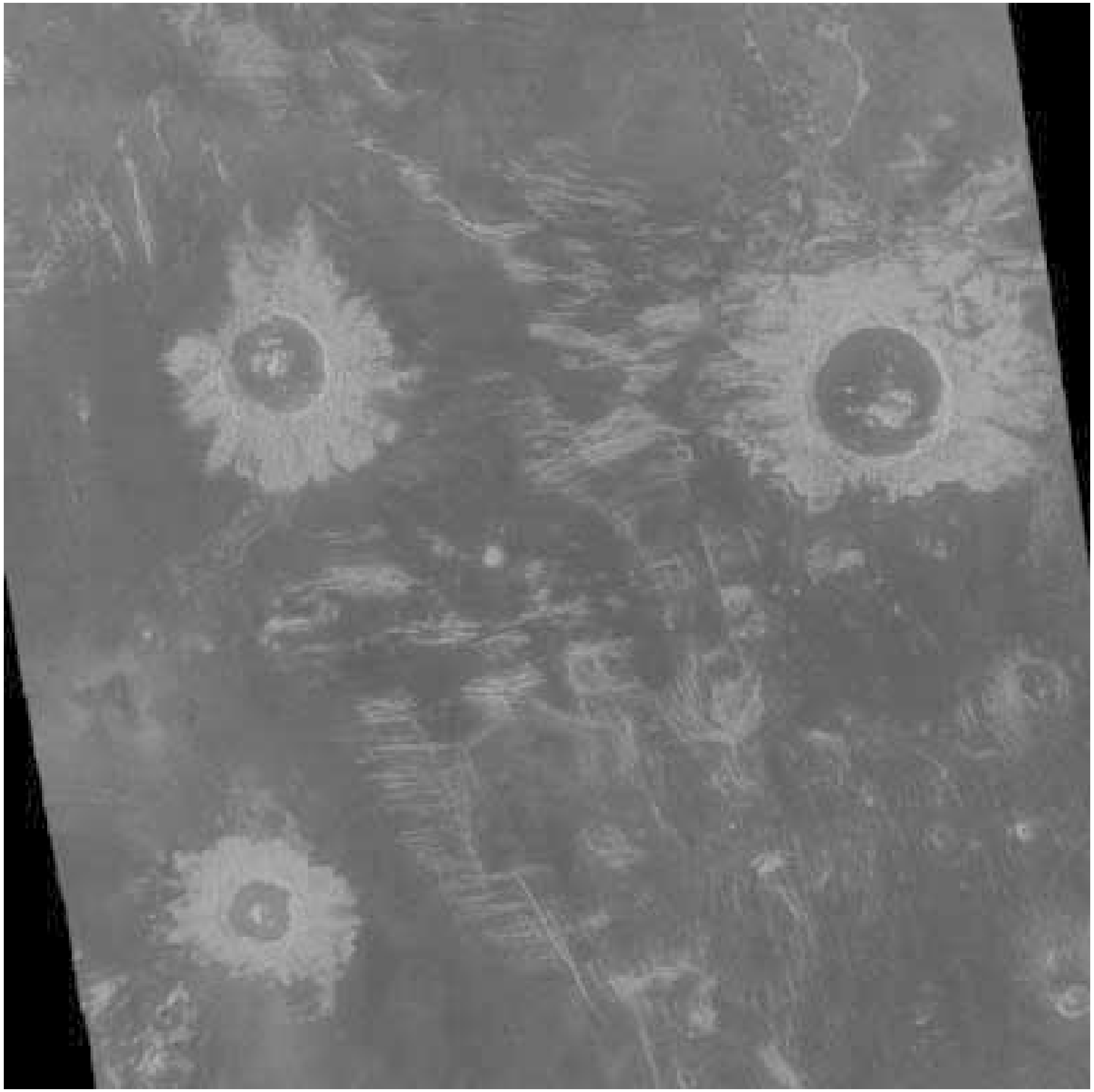

Venus, Magellan Spacecraft: Pancake Domes

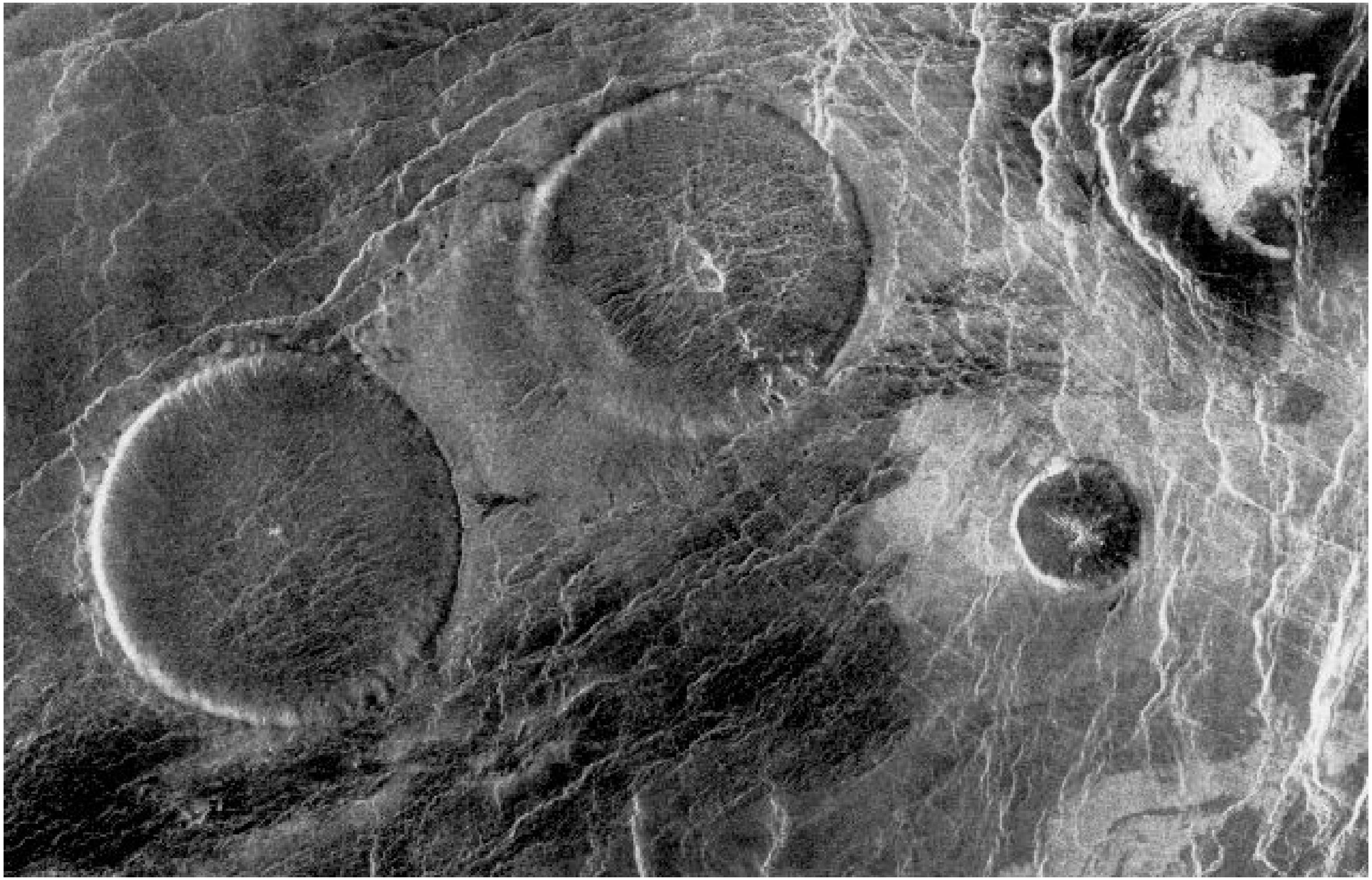

- Pancake domes formed from very viscous lava

Venus, Magellan Spacecraft: Corona

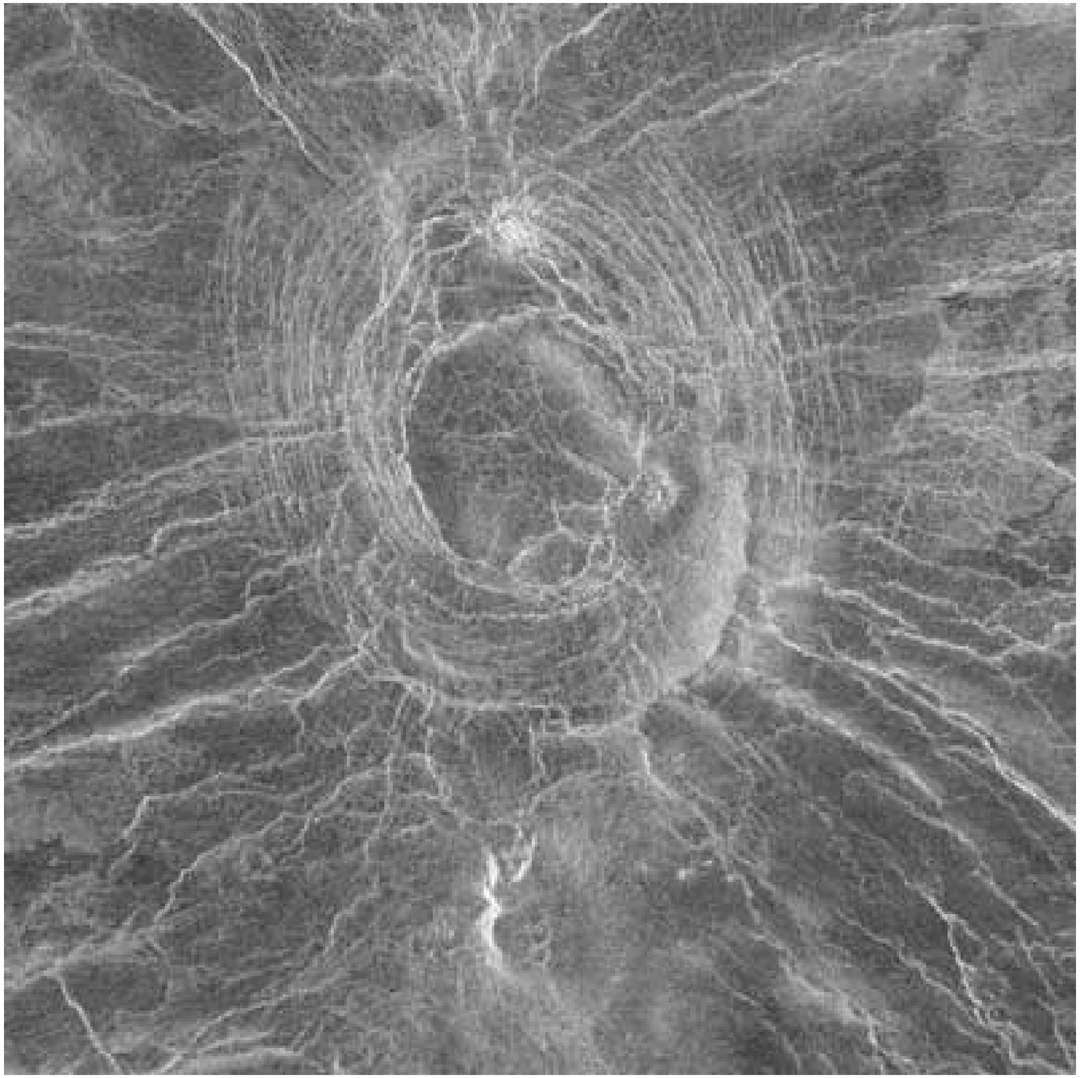

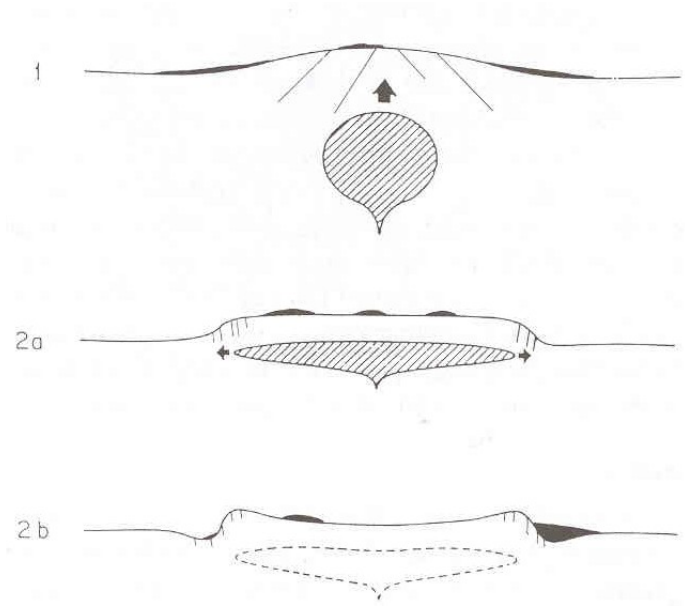

From Stofan et al. 1997 in Venus II

Active System

- Provide source of EM radiation you observe

- Send brief pulse (or sometimes "chirp")
- Control wavelength (frequency) and polarization of signal sent

- Observe some or all of following parameters of returned signal
  - Delay time of returned pulse(s): Gives distance of source
  - Direction from which signal returns: May determine "azimuthal spatial resolution"
  - Strength of returned signal: How well does target reflect signal?
  - Wavelength (Doppler) shift of returned signal: Speed of target
    - In "side scan radar" can also be used to provide enhanced azimuthal resolution
  - Polarization of returned signal: Scattering of light within target

Common Wavelengths

Name	Wavelength (cm)	Frequency (GHz)
K	0.8 – 2.4	40.0 – 12.5
X (3 cm)	2.4 – 3.8	12.5 – 8.0
C (6 cm)	3.8 – 7.5	8.0 – 4.0
S (8 cm, 12.6 cm)	7.5 – 15.0	4.0 – 2.0
L (23.5 cm, 25 cm)	15.0 – 30.0	2.0 – 1.0
P (68 cm)	30.0 – 100.0	1.0 – 0.3

$$v = \frac{c}{\lambda} = \frac{3 \times 10^8 \text{ m/s}}{\lambda}$$

Radar Overview

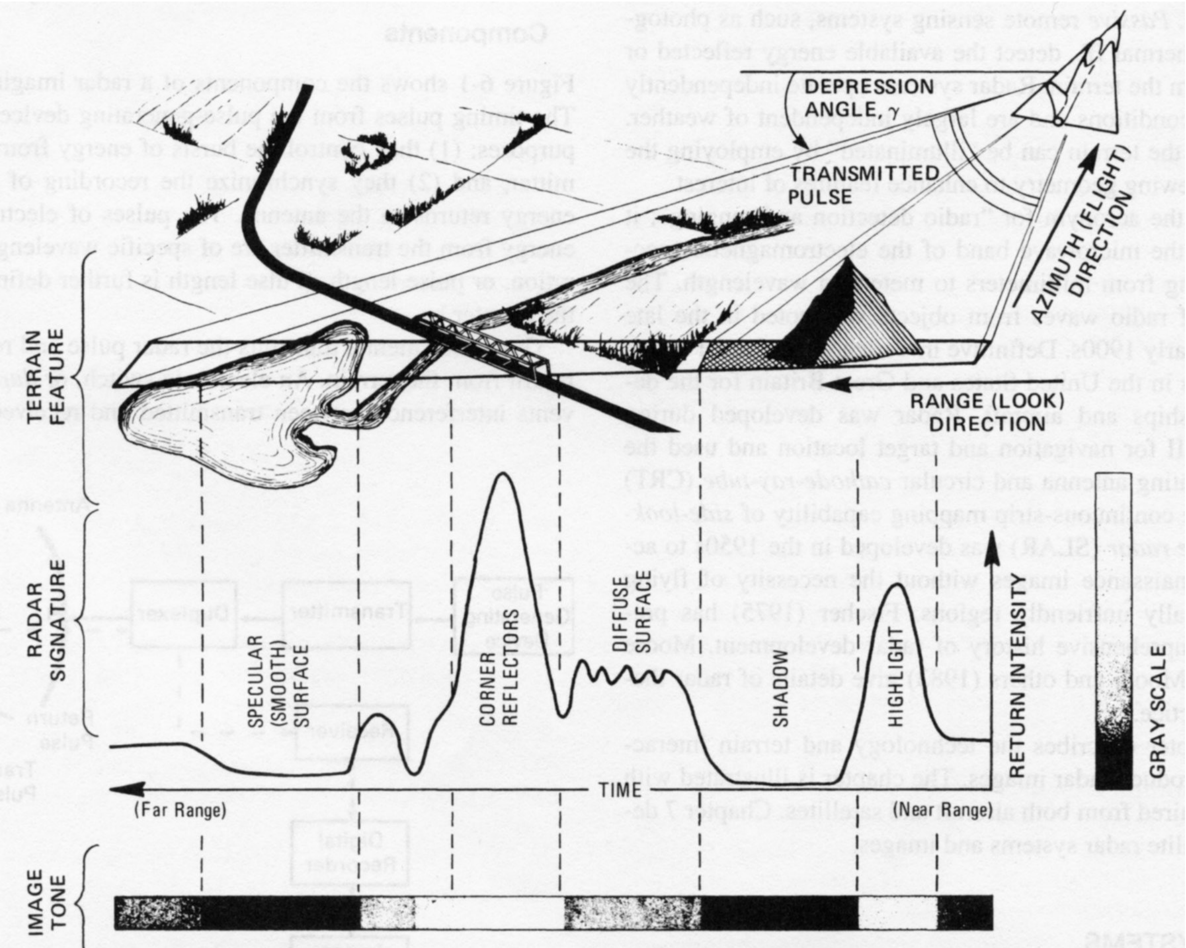

Figure 6-3 Terrain returns and image signatures for a pulse of radar energy.

- Highlights
- Shadows
- Diffuse surface
- Corner reflectors
- Specular (smooth) surface

Sabins Fig. 6-3

- Unusual geometry (often viewed “from side”)
- Unusual scattering mechanisms

Radar Typical Scene

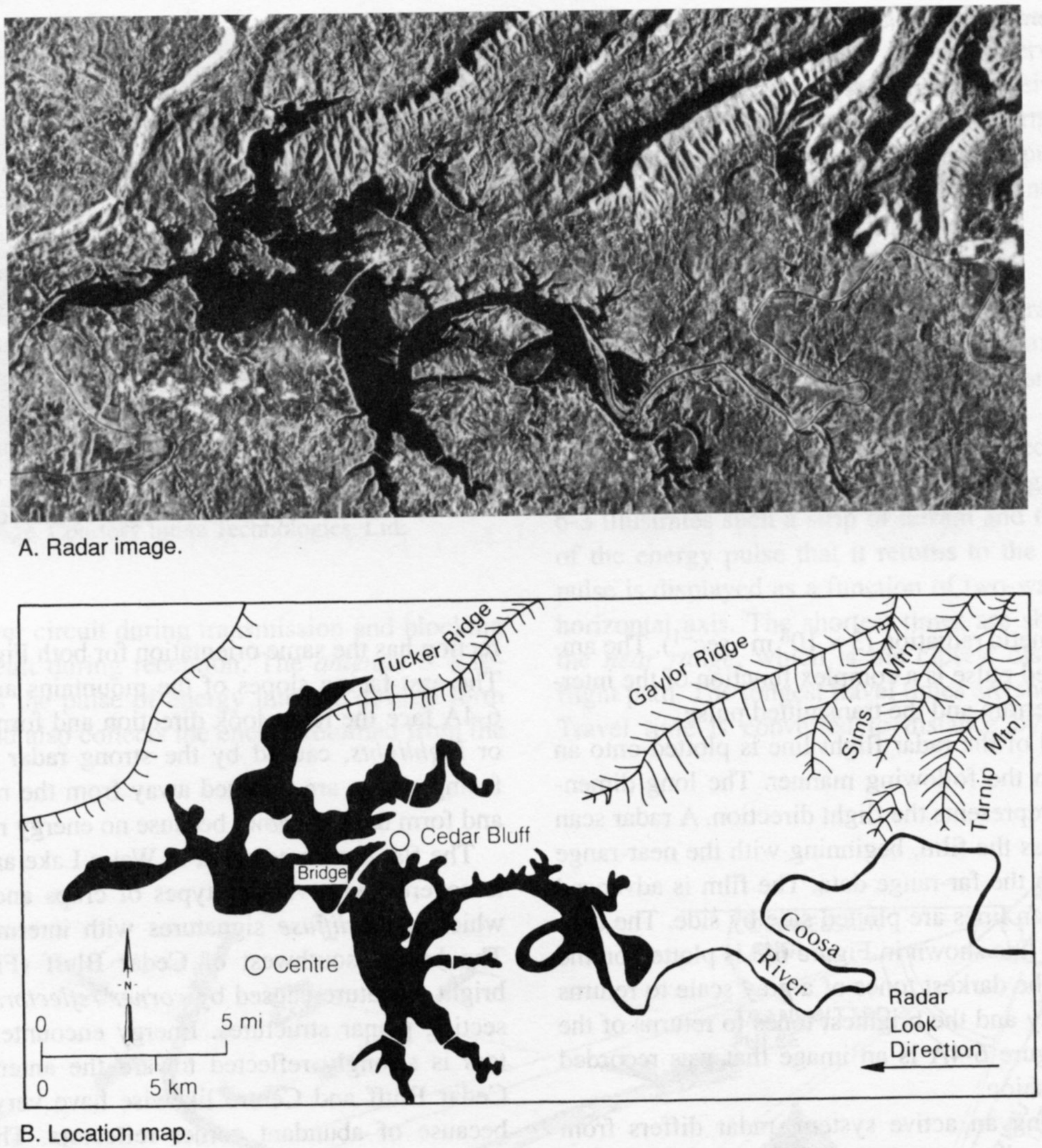

Figure 6-4 Radar image and map of Weiss Lake and vicinity, northeastern Alabama.

- Highlights: Near side of mtn.
- Shadows: Far side of mtn.
- Diffuse surface: Forest
- Corner reflectors: Bridge
- Specular (smooth) surface: Lake

Sabins Fig. 6-4

Radar Resolution: Real Antenna

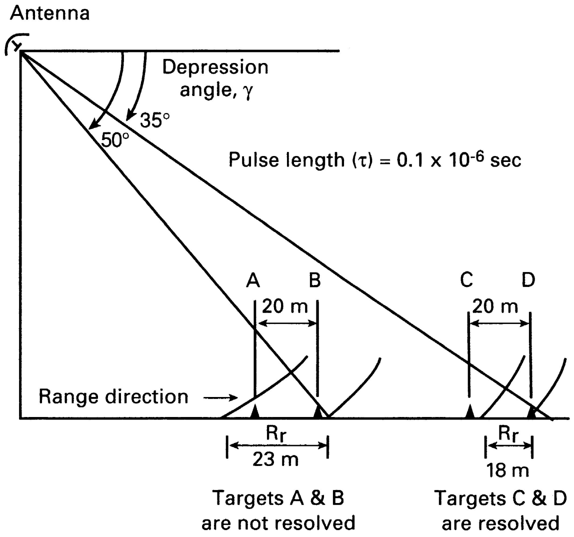

Figure 6-7 Range resolution for different depression angles.

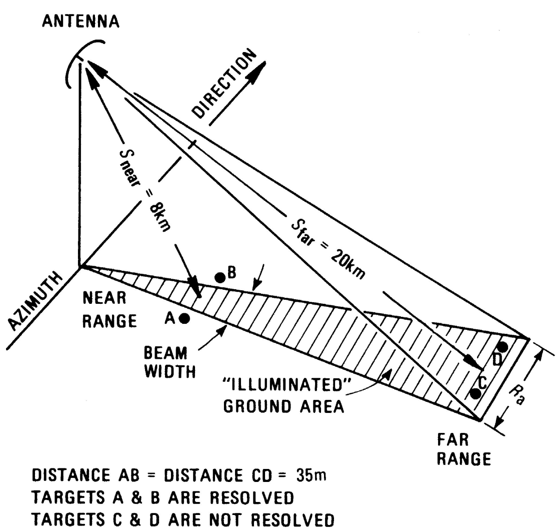

Figure 6-8 Azimuth resolution and beam width for a real-aperture system. From Barr (1969).

- Crosstrack = RANGE resolution: Set by pulse length

Radar Resolution: Real Antenna

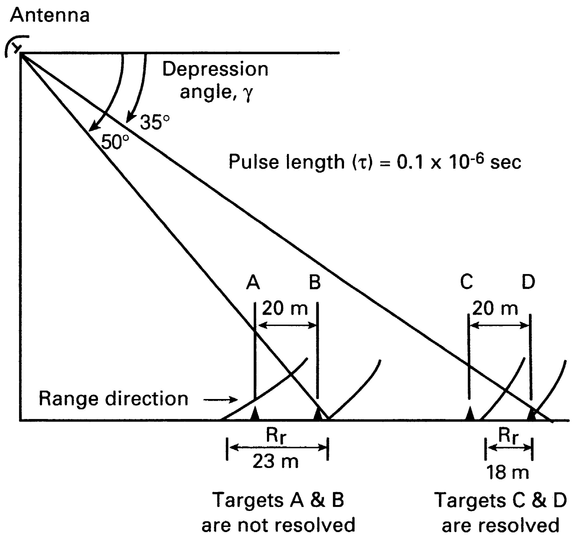

Figure 6-7 Range resolution for different depression angles.

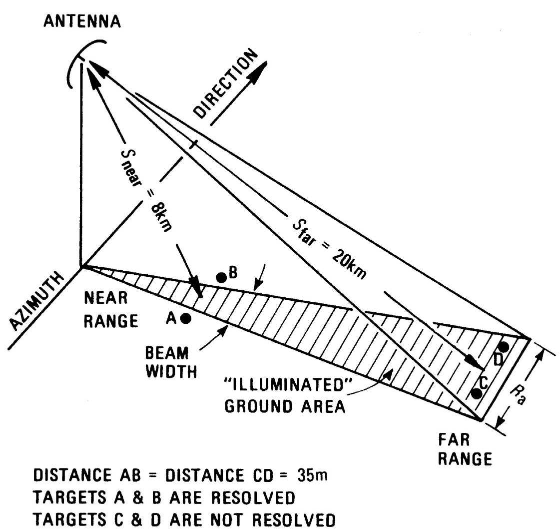

Figure 6-8 Azimuth resolution and beam width for a real-aperture system. From Barr (1969).

- "Radial" resolution:
  $\Delta r = c \times \Delta t / 2 = c\tau/2$

  For 0.1 μs pulse
  $\Delta r = 3\times10^{8}$ m/s $\times 0.1\times10^{-6}$ s / 2 = 15 m

- Crosstrack = RANGE resolution:
  in horizontal direction
  $R_r = (\tau c) / (2 \cos(\gamma))$
  15 m / cos(35°) = 18.3 m
  15 m / cos(50°) = 23.3 m

- Along-track – AZMUTHAL Resolution
  - Real Aperture – set by angular width of antenna pattern
  - $\theta \approx \lambda/D$
  - $R_a = S * (0.7\ \lambda/D)$
    S = slant range D = antenna length

- Synthetic aperture – related to Doppler resolution

Radar Resolution: Synthetic Antenna

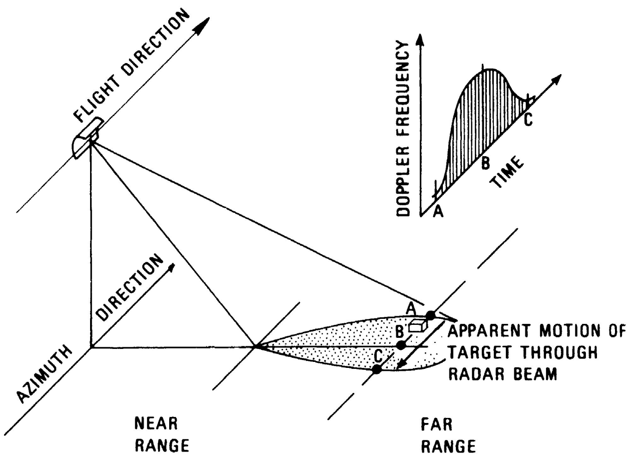

A. Shift in Doppler frequency caused by relative motion of target through radar beam.

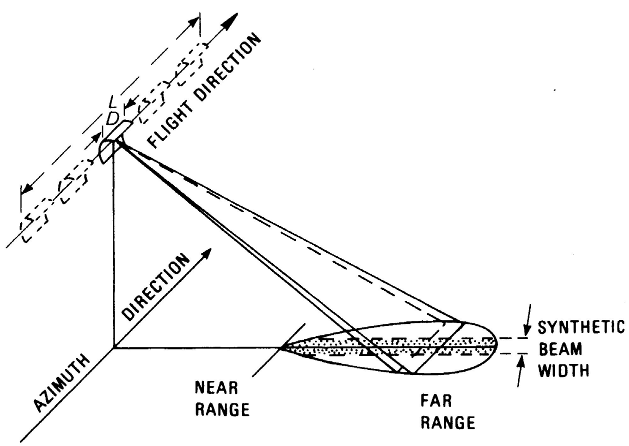

B. Azimuth resolution of synthetic-aperture radar. The physical antenna length *D* is synthetically lengthened to *L*.

Figure 6-9 Synthetic-aperture radar system. From Craib (1972, Figures 3 and 5).

- Two different kinds of "synthetic aperture synthesis"
- Use "Doppler Effect"
- Record and "electrically" combine signals from radar at different positions to make longer effective antenna
  - Need "phase" information, so doesn't work with visible light

Scattering Geometry

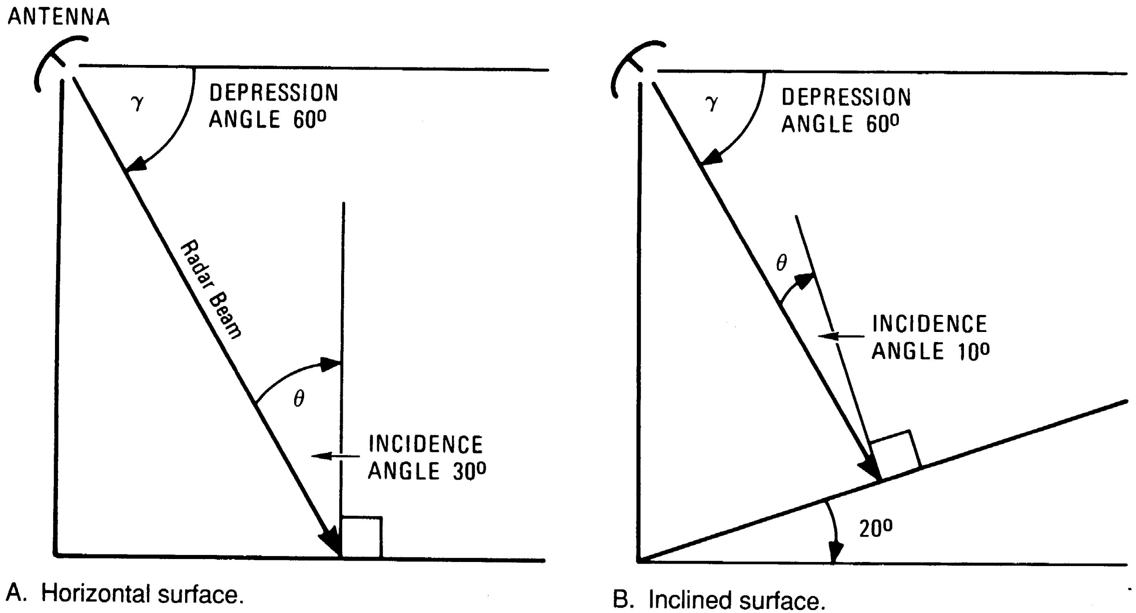

Figure 6-5 Depression angle and incidence angle.

- Amount of energy sent back to receiver depends on:
  – incidence angle
  – degree of scattering in target

Stealth Aircraft avoid right angles

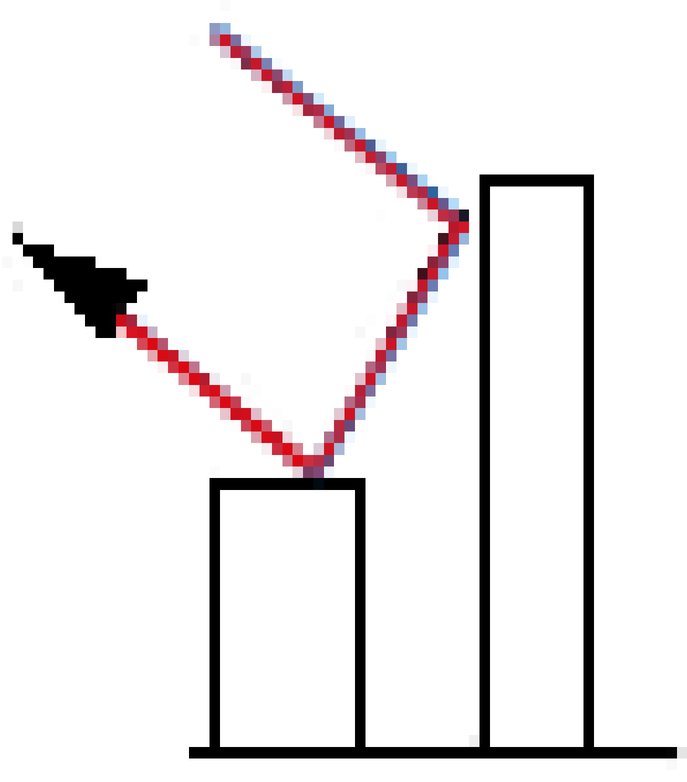

Sabins

Look direction also important in geology

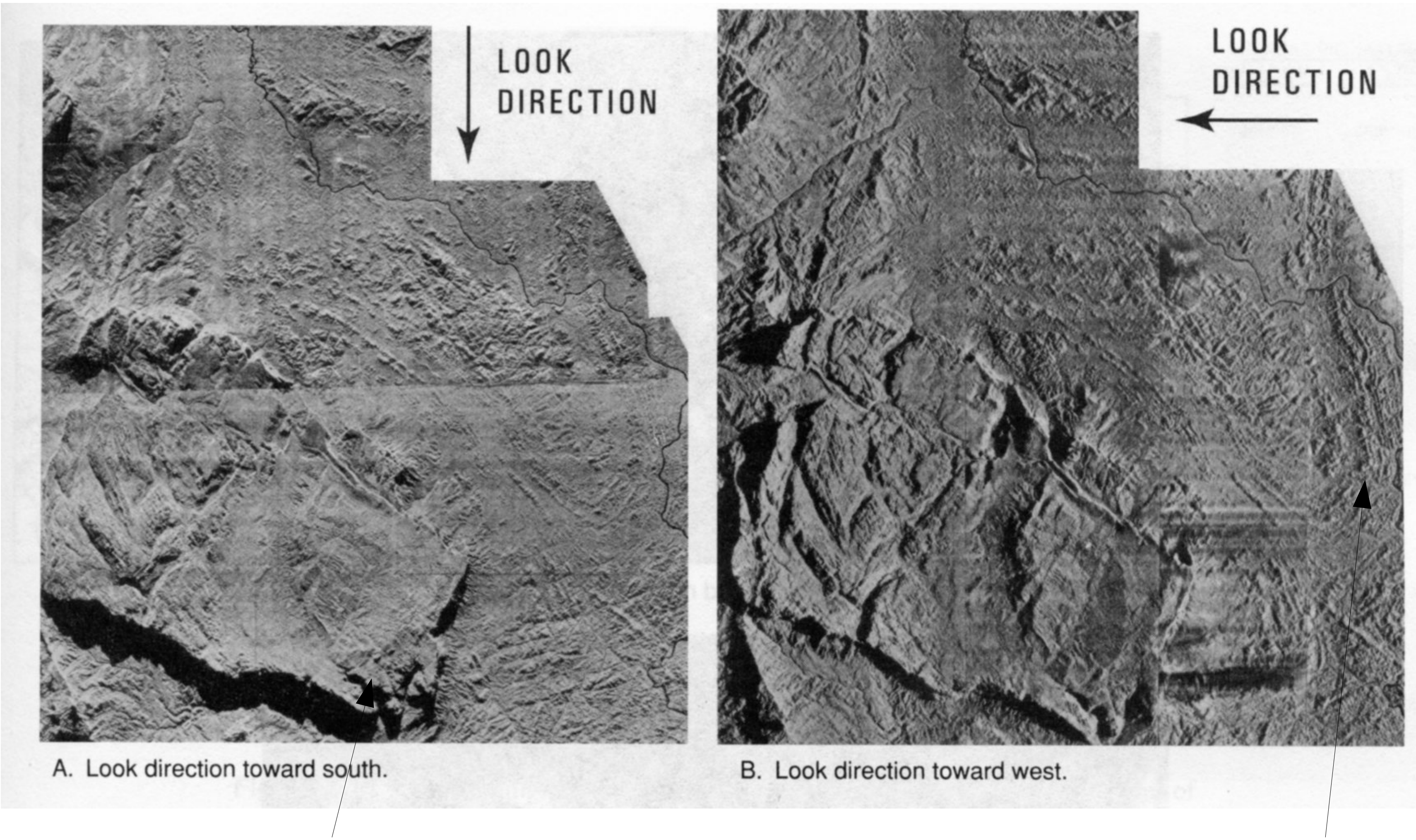

A. Look direction toward south.

B. Look direction toward west.

Sabins Fig. 6-12 pg. 187

Multiple Reasons for Dark or Bright Returns

- Dark Returns
  - Flat surface of high reflectance (energy reflects away)
  - Areas sloping away from flight path are shadowed
  - Area of low reflectance (energy is absorbed)

- Bright Returns
  - Flat surface of high reflectance perpendicular to beam
  - Strong dihedral angle reflectors (multiple reflections)
  - Rough areas of high reflectance

- Will return to "Radar Returns" after covering geometry

Shadowing

Shadowing occurs because tall objects do not allow the low-angle radar beam to illuminate the area on steep slopes facing away from the flight path.

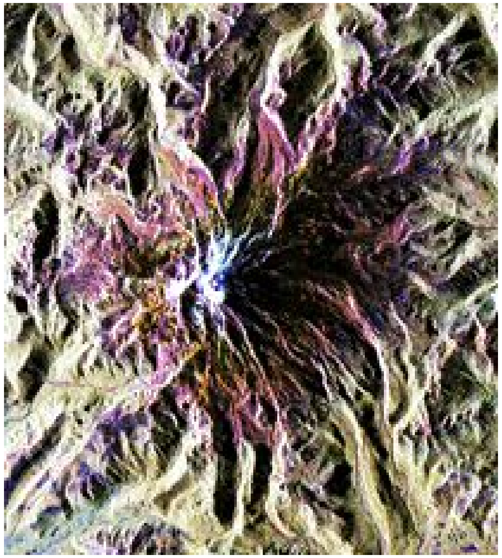

Mt. Rainier

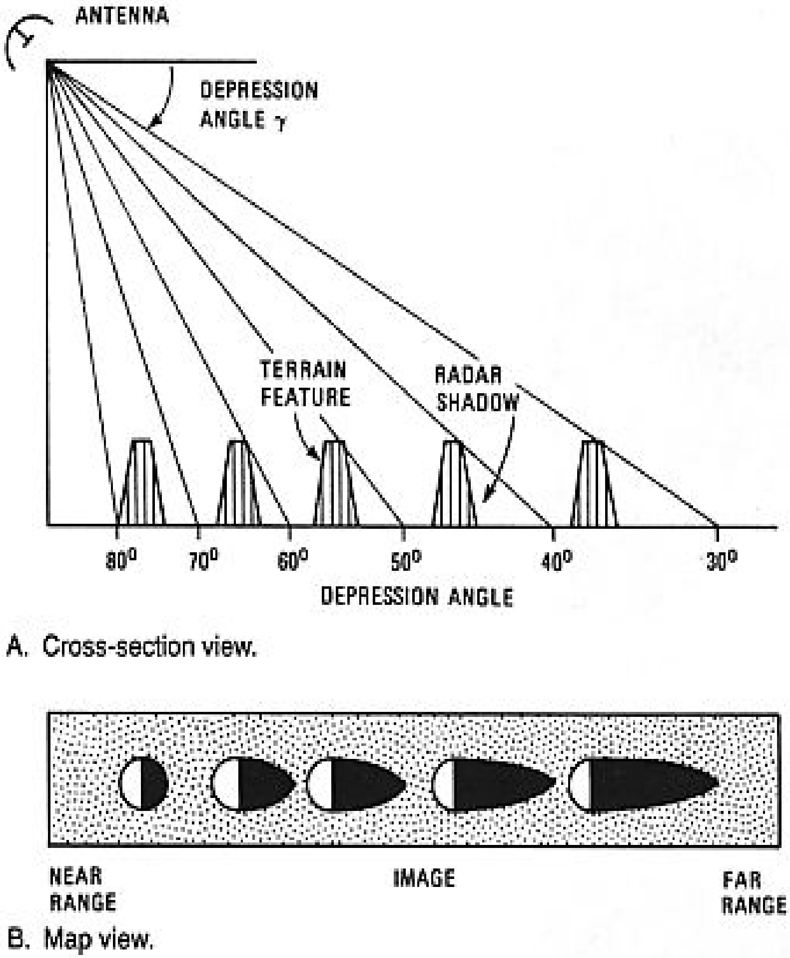

Distortions of Radar Images: Foreshortening

Foreshortening (like layover) is due to the return from the top of a tall object coming too soon.

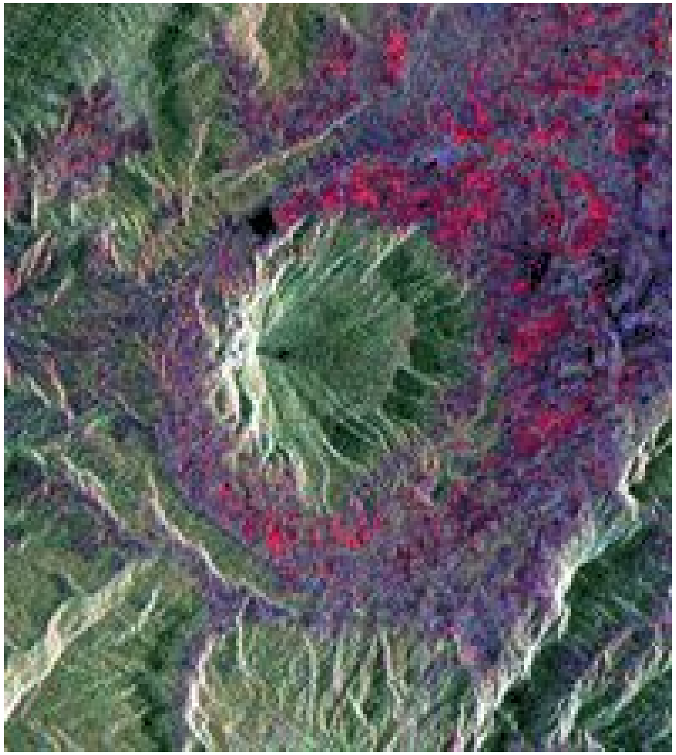

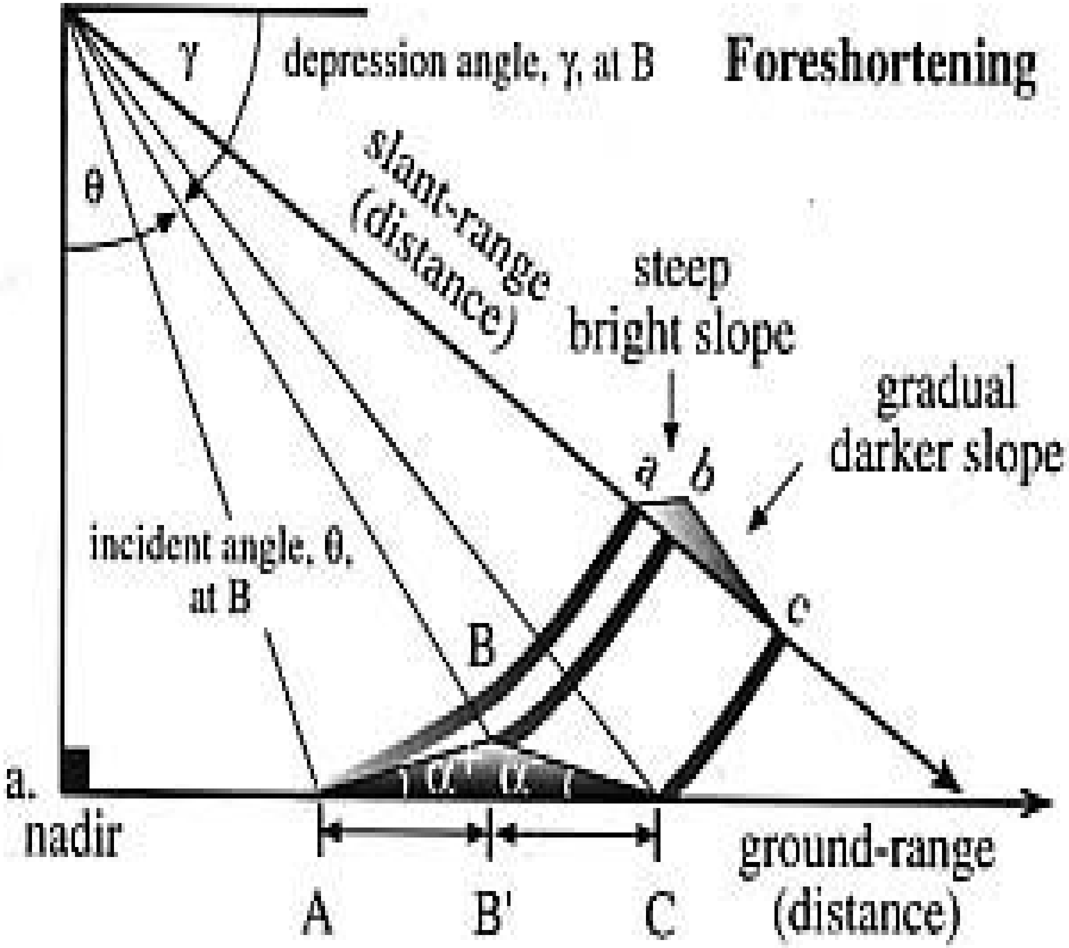

Distortions of Radar Images: Layover

Layover is caused by the return from the top of the peak coming in before or at the same time as the return from the base.

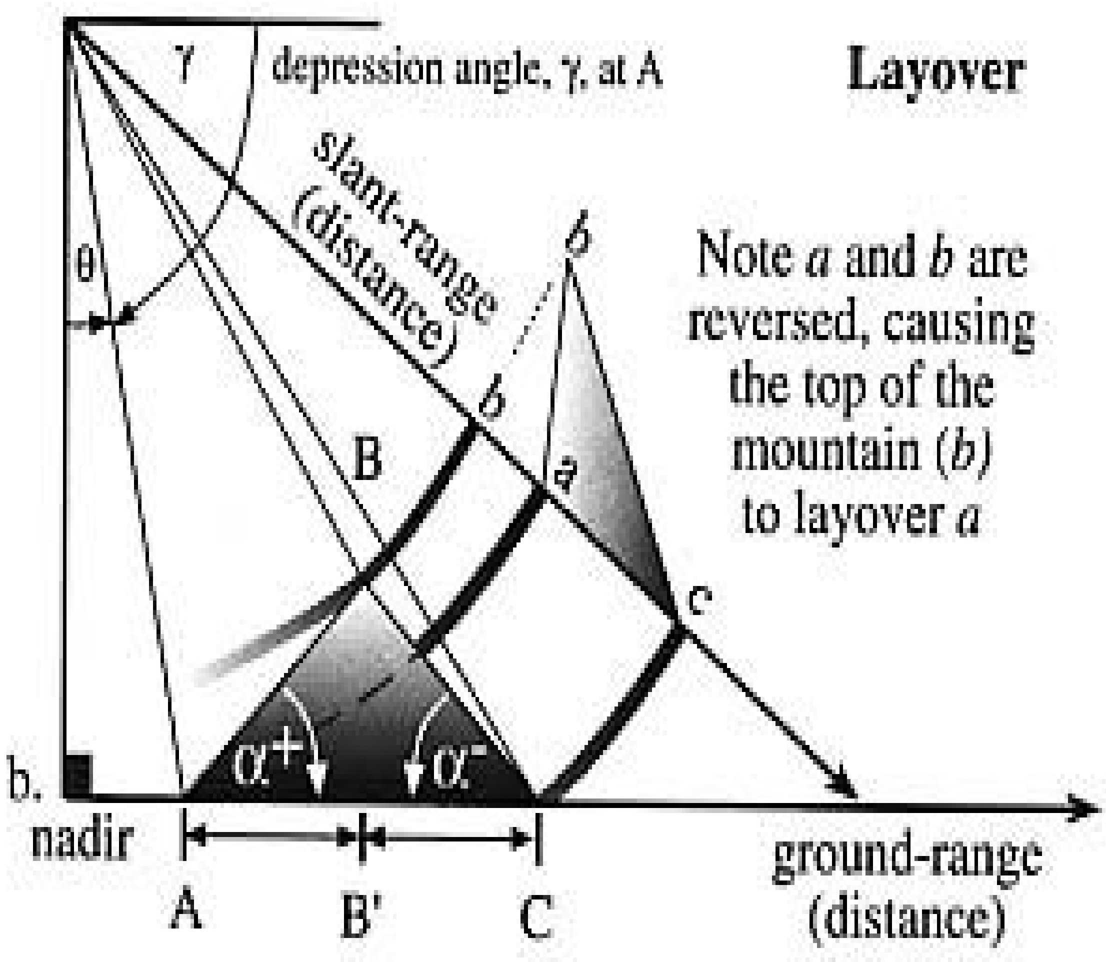

Two depression angles (i.e. 2 offset passes) can produce stereo radar

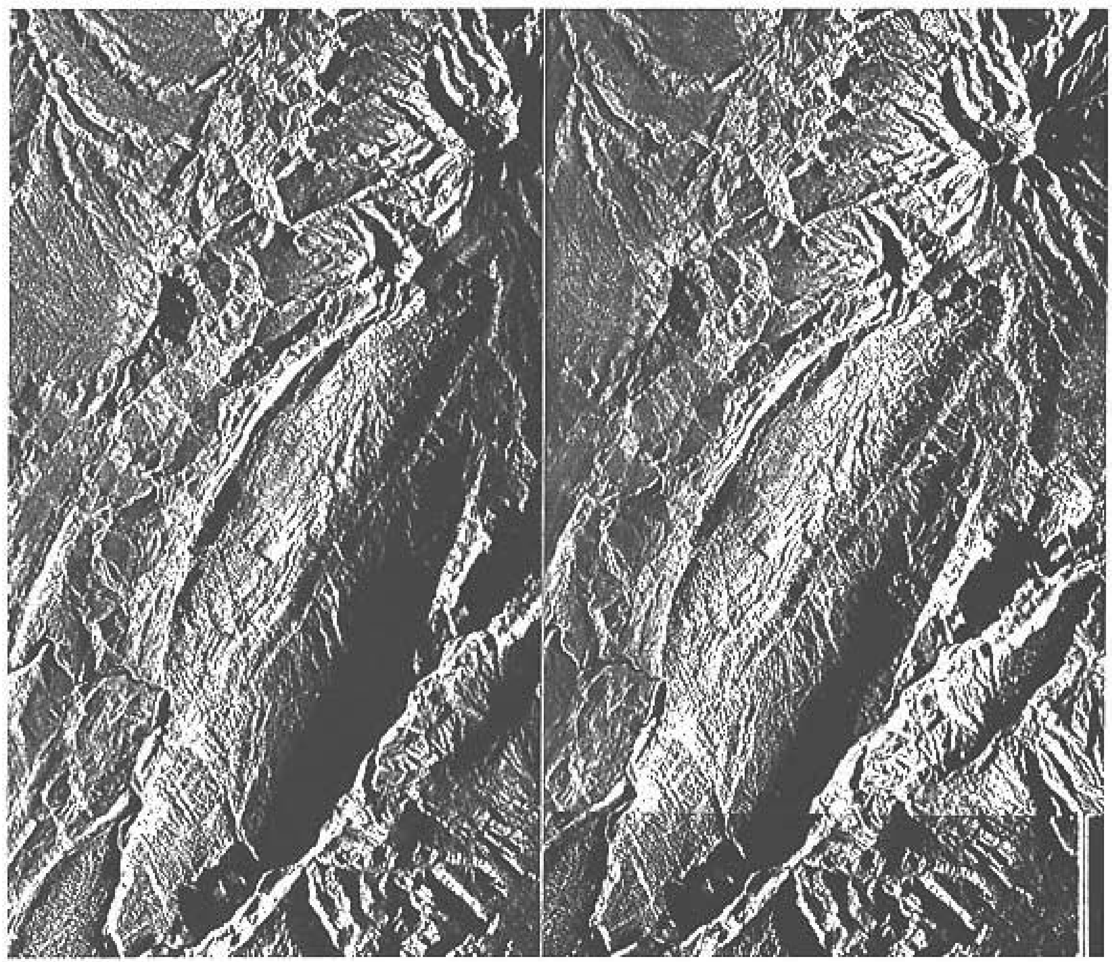

A. Left image. B. Right image.

Polarization Images

- Transmit Receive
  - HH parallel polarized
  - HV cross polarized
  - VV parallel polarized
  - VH cross polarized

- Single reflection:
  - Preserves linear polarization
  - Reverses clockwise or counterclockwise sense
  - Produces stronger return for E in plane of surface

- Multiple oblique reflections (volume scattering) depolarize returned signal

From our text by Sabins

Radarsat-2: North end of Sermilik fjord, Greenland

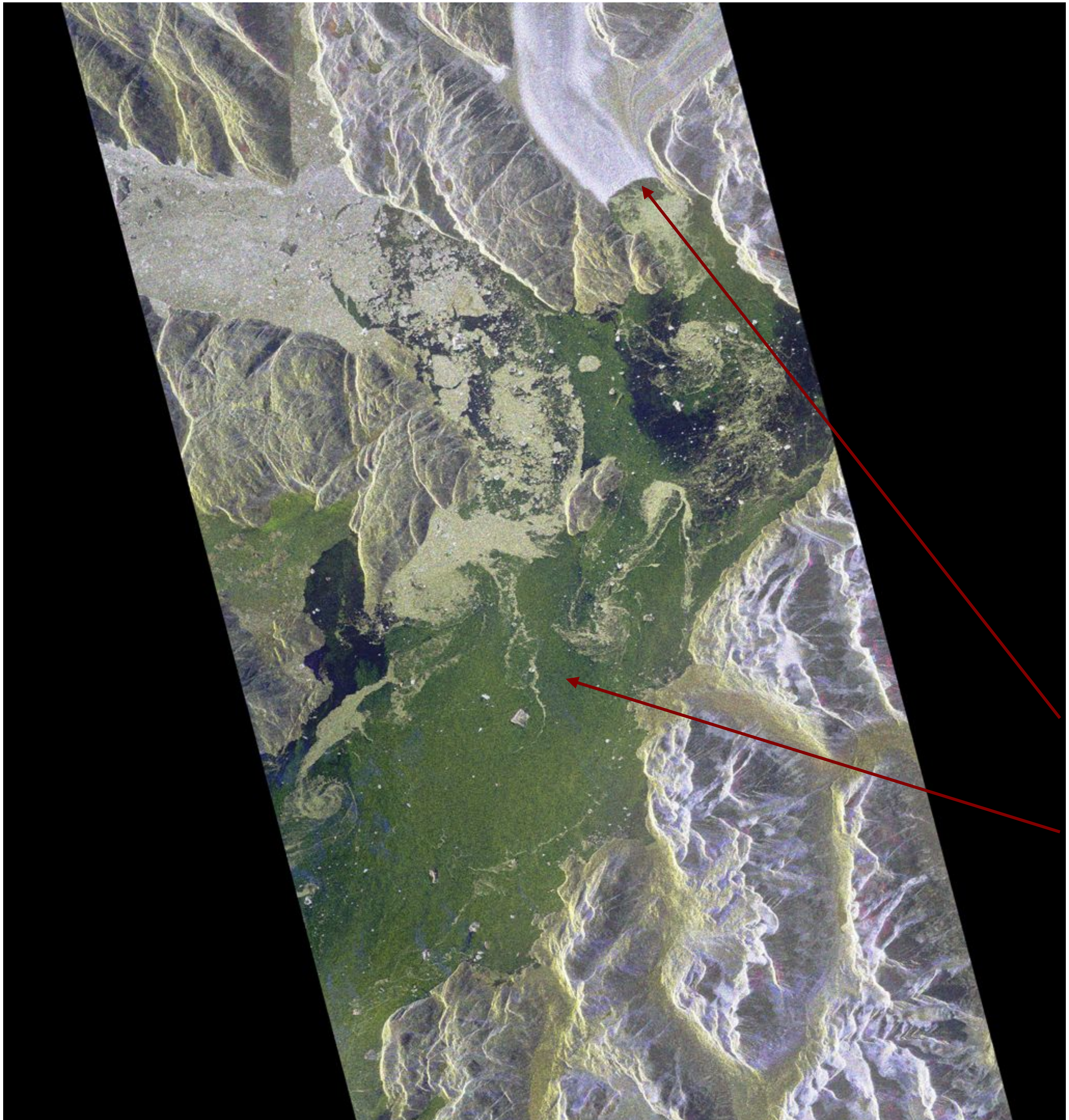

RGB = (HH, V V, HV)

25km x 50km

25m resolution

Fenrisgletscher glacier

Fjord, with different types of sea ice and leads (open water)

Radar Interacts with Volumes

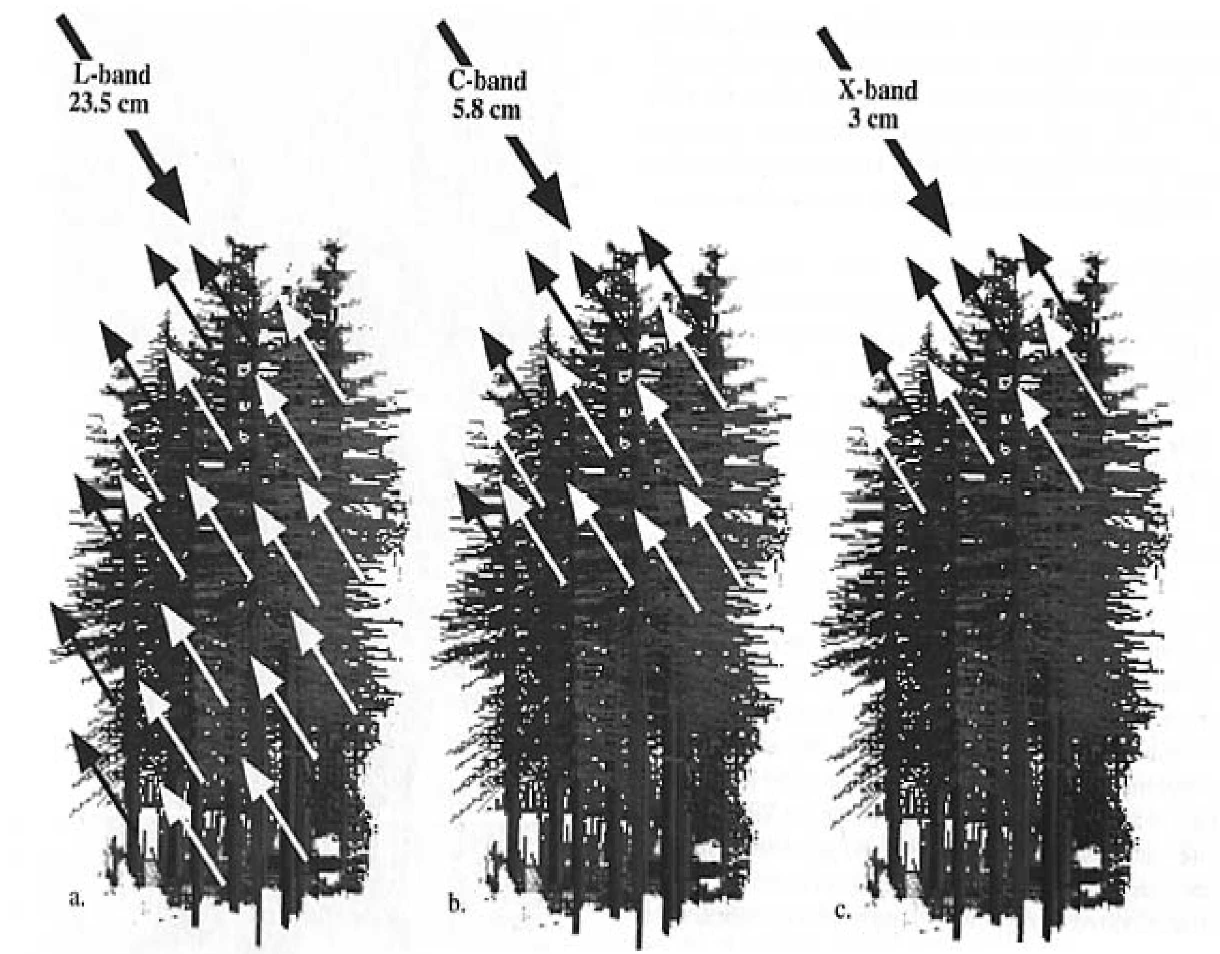

Because of substantial penetration the returns from most materials represent a volume interaction.

Interferometry

- Normally Range resolution determined by length of pulse:
  - $R_r = (\tau c) / (2 \cos(\gamma))$ where τ = pulse time, γ = depression angle
  - Occurs because you compare time of pulse return
  - Pulses should not overlap (much) to resolve targets

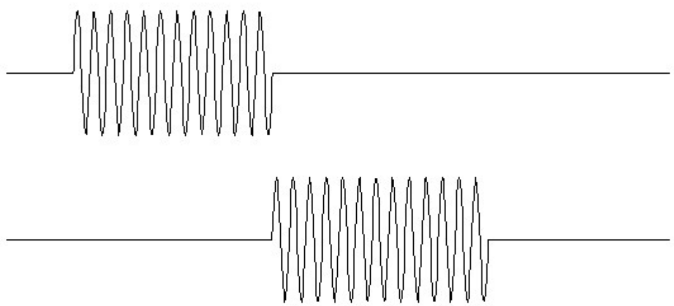

- With interferometry, compare phase of wave, not time of pulse
  - Resolution si

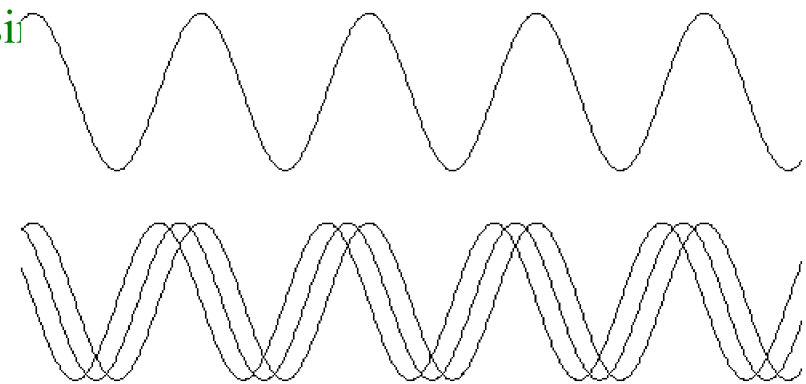

Interferometry

- Can measure distances to a fraction of a wavelength
- Often used to measure changes in distances between measurements taken at two different times
  - Earthquake fault motion
  - subsidence
  - glacier/ice sheet motion

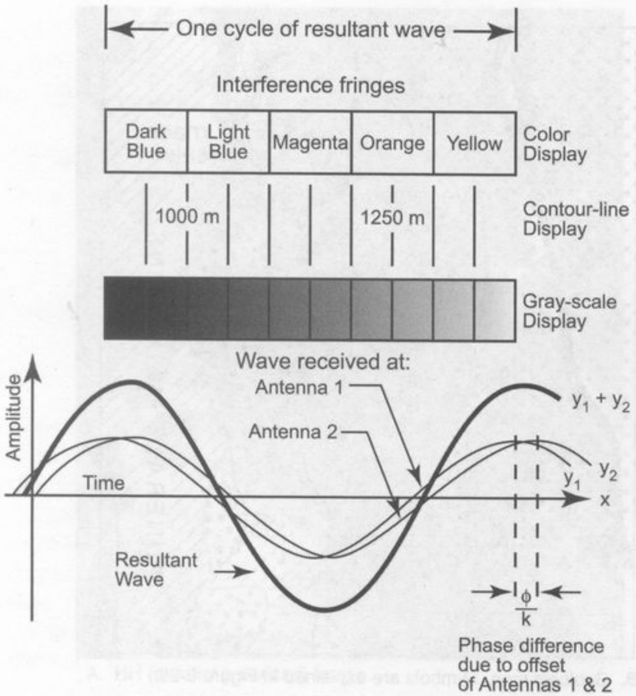

Figure 6-40 Diagram showing origin of interference fringes from two received radar waves that are not in phase.

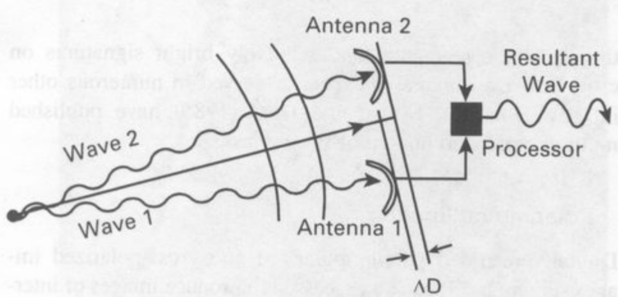

Figure 6-41 Radar interferometer system. Only one antenna transmits the radar wave. The return waves are received by two antennas that are spaced at different distances from the target; therefore, the two return waves are not in phase. Interference results when the two return waves are combined by the processor.

From our text by Sabins

Long Valley Caldera

- Very large eruptions in distant past
- Evidence in magma emplacement underground

A. Radar image used in interferogram.

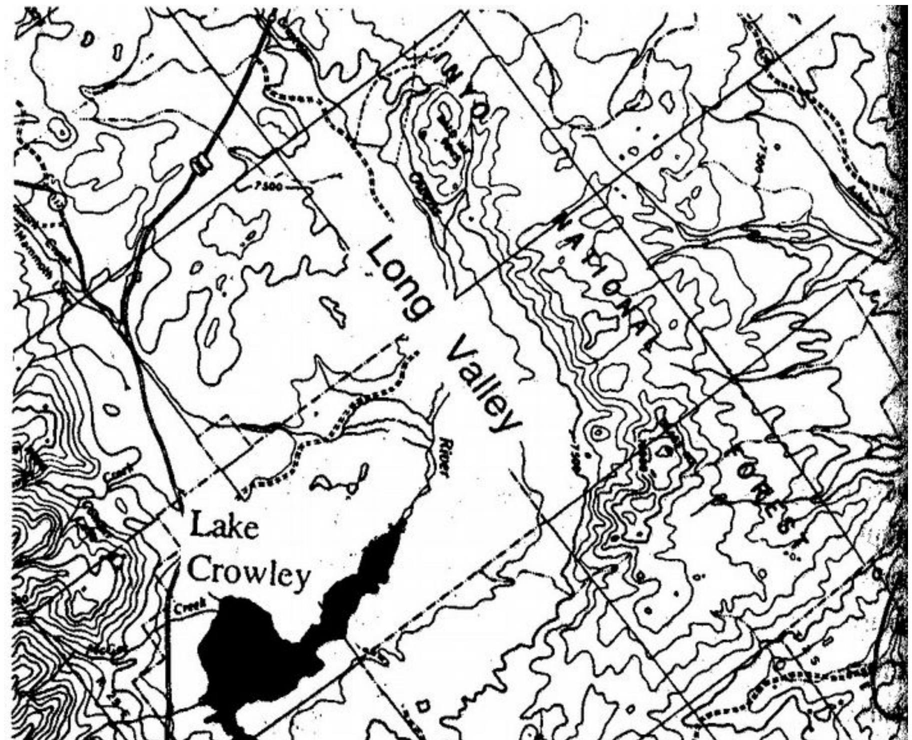

B. Conventional topographic map from aerial photographs.

Figure 6-42 Radar image and map, Long Valley, California.

From our text by Sabins

Long Valley Caldera

- Each “fringe” usually a shift of λ/4
- Not entirely clear from Sabins how this has been processed
- Better examples in lab and later lectures

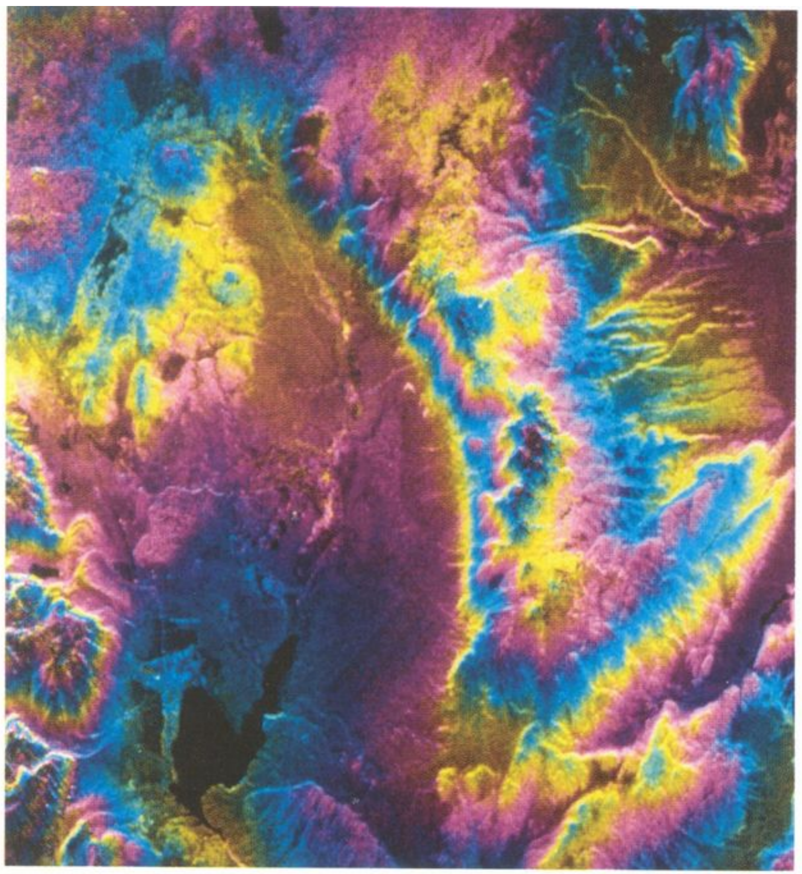

A. Interferogram, Long Valley, California.

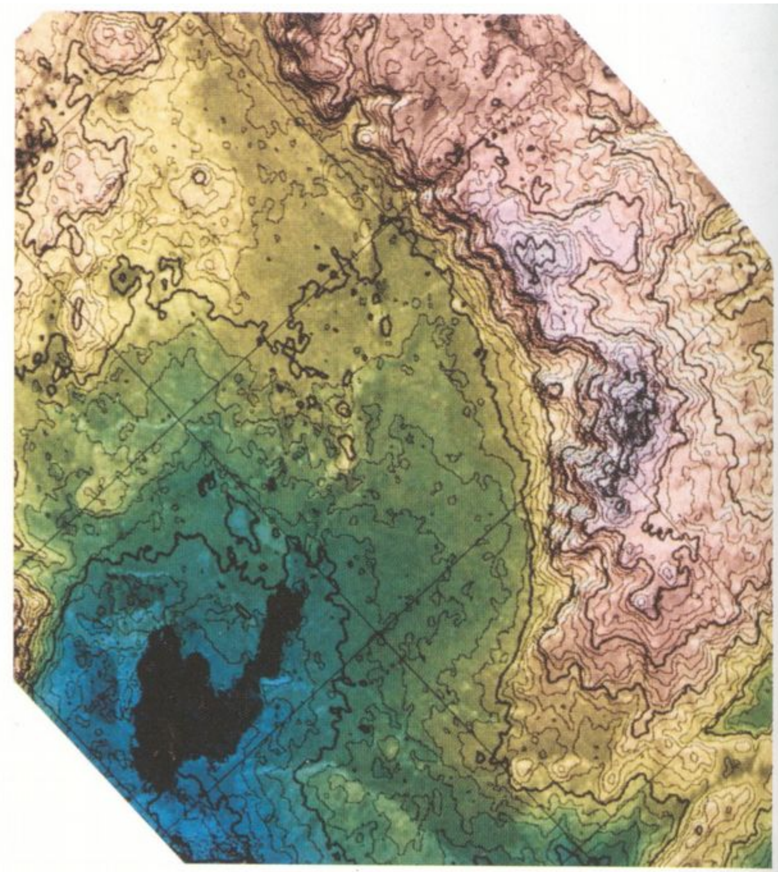

B. Topographic map from interferogram, Long Valley, California.

From our text by Sabins

Dike injection on Kilauea NE rift zone

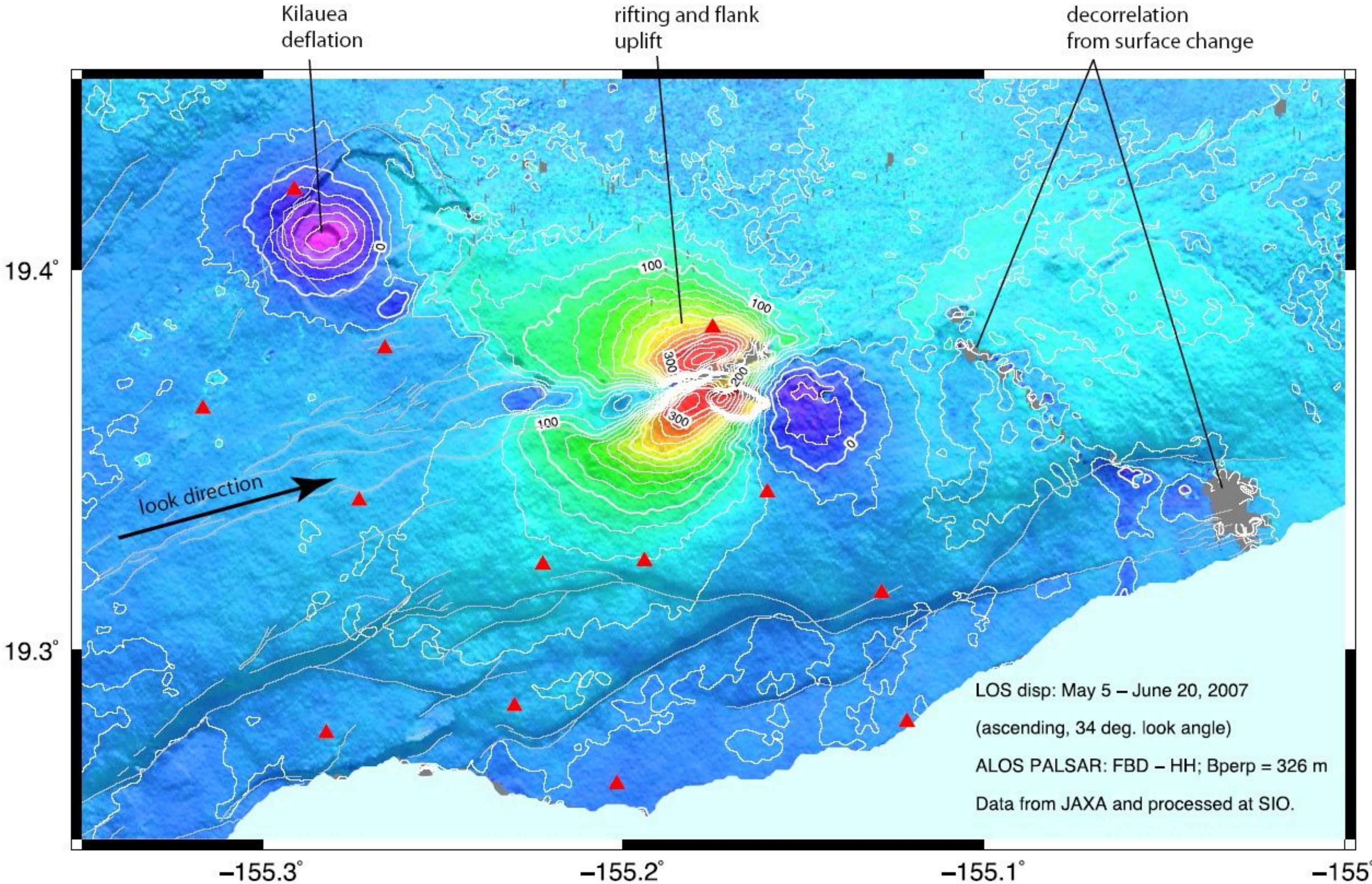

Radar interferogram constructed from ALOS PALSAR acquisitions on May 5 and June 20 (day 171, 8:52 GMT). This time period spans most of the "Fathers Day" (June 17) rift event. These data were acquired in the fine beam dual polarization mode (FBD-HH, 14 MHz). Correlation is high even in forested areas and the phase was unwrapped and scaled to line-of-sight millimeters (LOS). The radar look direction is from the WSW and 34° from vertical. GPS receivers with continuous vector measurements are marked by red triangles.

PALSAR 2007 May 5 vs. June 20 difference. Contours are LOS (line-of-site) mm
From "ascending" passes – looking along the rift

Dike injection on Kilauea NE rift zone

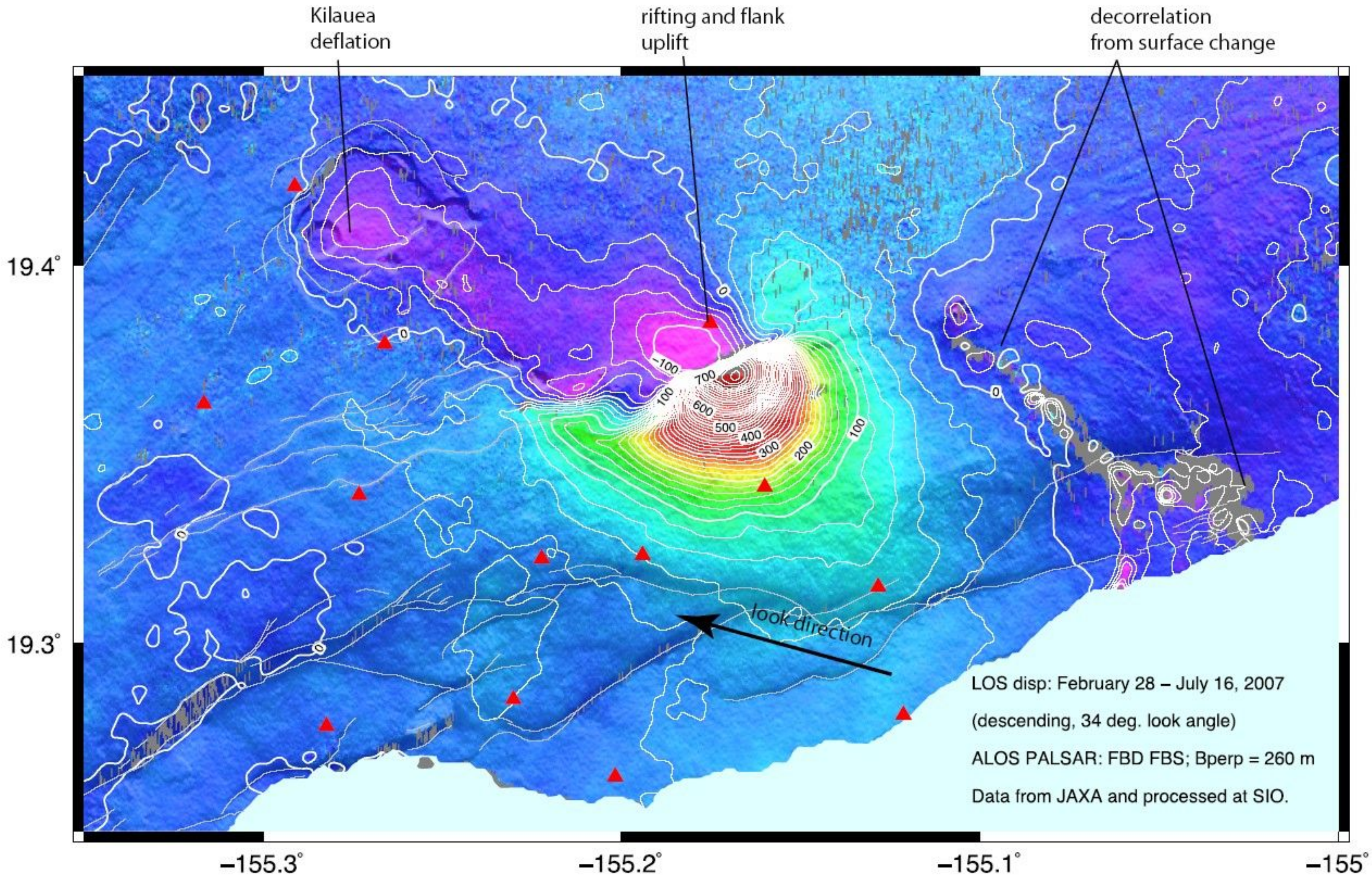

Radar interferogram constructed from ALOS PALSAR acquisitions on Feb 28 and July 16 (8:52 GMT). This time period spans the "Fathers Day" (June 17) rift event. These data were acquired two modes. The Feb 28 acquisition was FBD-HH (14 MHz) while the July 16 acquisition was FBS (28 MHz) the raw FDB data were interpolated to the higher FBS sampling rate. The radar look direction is from the ESE and 34° from vertical.

PALSAR 2007 Feb. 28 vs. July 16 difference. Contours are LOS (line-of-site) mm
From "descending " passes – with component perpendicular to rift. Rift flanks rise and separate.

Roughness Criteria

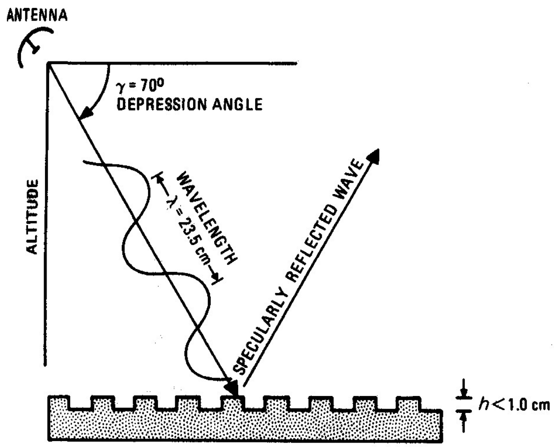

A. Smooth surface, no return.

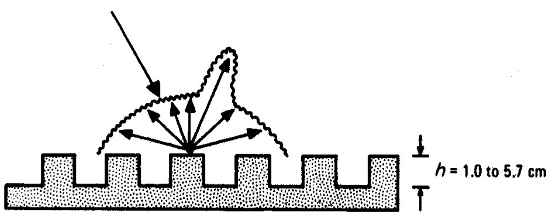

B. Intermediate relief, intermediate return.

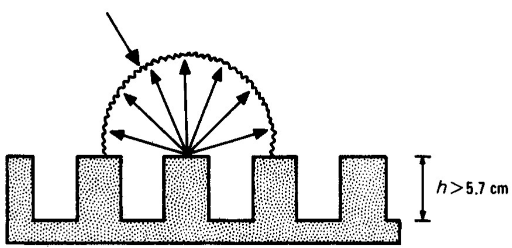

C. Rough surface, strong return.

Figure 6-31 Models of surface roughness criteria and return intensity for radar images at 23.5-cm wavelength.

- Rayleigh criterion
  smooth if $h < \lambda / (8 \sin \gamma)$

- Peake and Oliver define
  3 categories:

  smooth: $h < \lambda / (25 \sin \gamma)$
  rough: $h > \lambda / (4.4 \sin \gamma)$
  intermediate: h between above

For $\gamma = 40^o$

	X (3 cm)	C (6 cm)	L (23.5 cm)
Smooth: h<	0.19 cm	0.37	1.46 cm
Rough: h>	1.06 cm	2.12 cm	8.31 cm

From our text by Sabins

Roughness Criteria

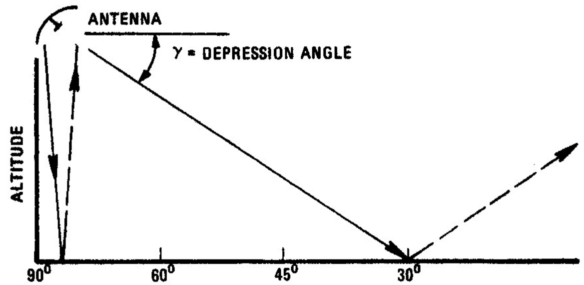

A. Smooth surface with specular reflection.

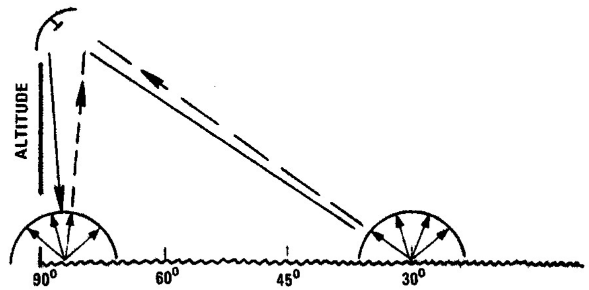

B. Rough surface with diffuse scattering.

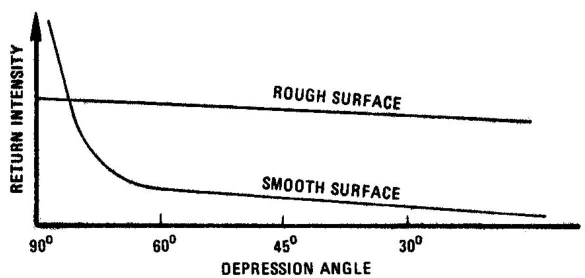

C. Return intensity as a function of depression angle.

Figure 6-32 Radar return from smooth and rough surfaces as a function of depression angle.

- Rayleigh criterion
  smooth if $h < \lambda / (8 \sin \gamma)$
- Peake and Oliver define
  3 categories:

smooth: $h < \lambda / (25 \sin \gamma)$
rough: $h > \lambda / (4.4 \sin \gamma)$
intermediate: h between above

For $\gamma = 40^{o}$

	X (3 cm)	C (6 cm)	L (23.5 cm)
Smooth: h<	0.19 cm	0.37	1.46 cm
Rough: h>	1.06 cm	2.12 cm	8.31 cm

From our text by Sabins

Backscatter Coefficient: σ

Isotropic Scattering
(equal in all directions)

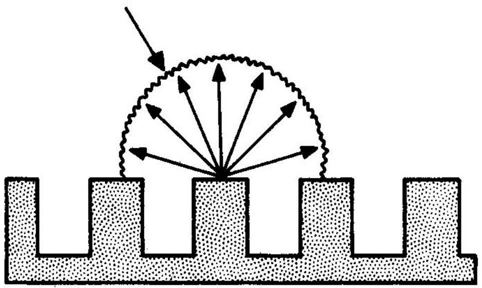

Non-isotropic Scattering

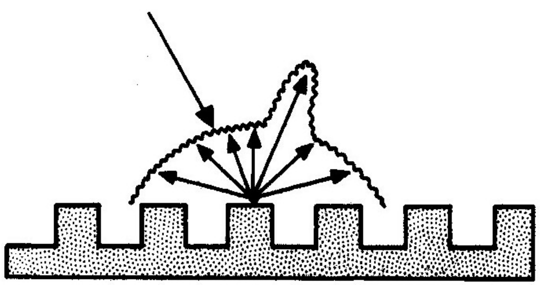

From our text by Sabins

$$\sigma = 10\log\left(\frac{\text{Energy received}}{\text{Energy expected from isotropic scatterer}}\right) \quad \text{dB} \quad \text{(i.e. decibels)}$$

$$\sigma = 10\log(1) = 10\,(0) = 0\text{ dB} \quad \text{Isotropic}$$

$$\sigma = 10\log\left(\tfrac{1}{10}\right) = 10\,(-1) = -10\text{ dB} \quad \text{Lower figure}$$

$$\sigma = 10\log\left(\tfrac{1}{100}\right) = 10\,(-2) = -20\text{ dB}$$

$$\sigma = 10\log(10) = 10\,(+1) = +10\text{ dB} \quad \text{Corner cube - like}$$

$$\frac{\text{Energy Received}}{\text{Energy expected from isotropic scatterer}} = 10^{\sigma/10}$$

Note: Use $\log_{10}(\ )$, not $\ln(\ ) = \log_e(\ )$

Death Valley Alluvial Fans


Devils Golf Course
Death Valley National Park
California
Crystallized salts compose the jagged formations of this forbidding landscape. Deposited by ancient salt lakes and shaped by winds and rain, the crystals are forever changing.
Listen carefully. On a warm day you may hear a metallic cracking sound as the salt pinnacles expand and contract.
The Death Valley saltpan is one of the largest protected saltpans in North America. Salt continues to be deposited by recurring floods that occasionally submerge the lowest parts of the valley floor.
Delicate salt formations (right) are hidden among the harsh and rigid spires. Close inspection may reveal the tiny salt structures. Take care—one curious touch can cause them to crumble.
Be careful! Walking on the Devils Golf Course is very difficult. A fall could result in painful cuts or even broken bones.

Roughness at Copper Canyon

X Band (3.0 cm)

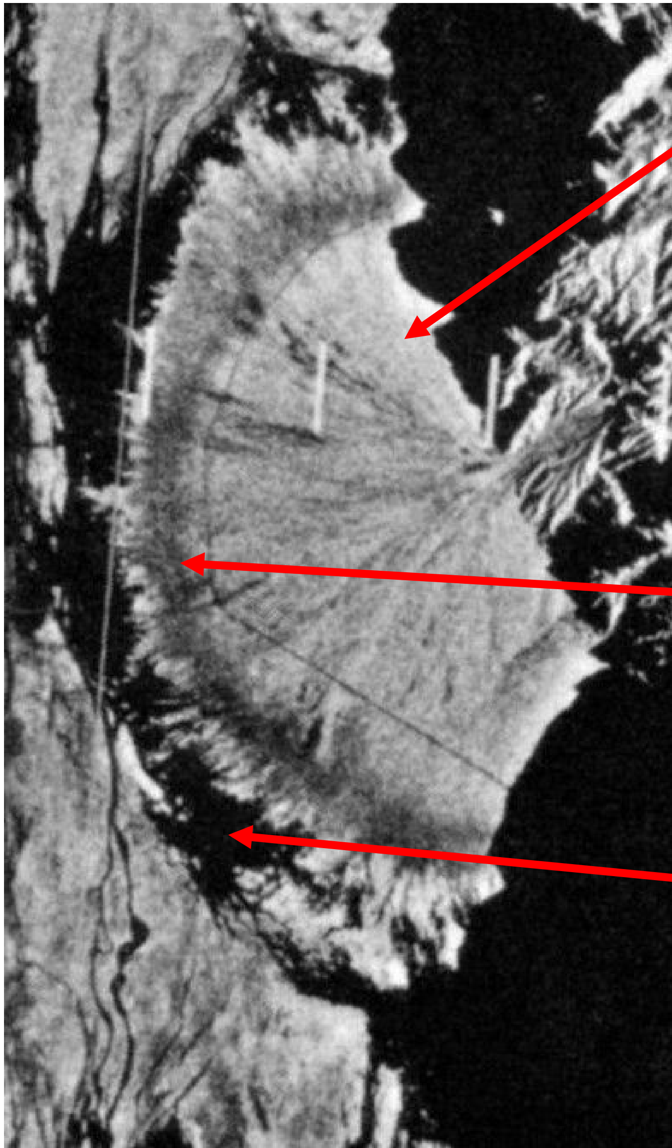

Sabins Fig. 6-36 a (pg. 206)

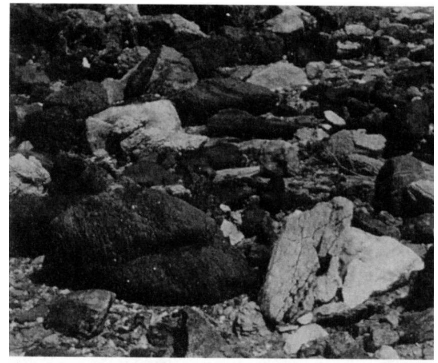

A. Coarse gravel, $h = 12.0$ cm.

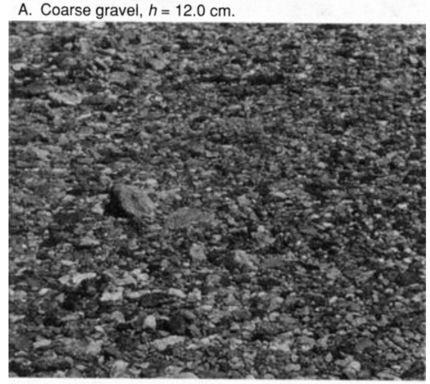

E. Desert pavement, $h = 1.0$ cm.

F. Floodplain deposits, $h = 0.2$ cm.

Smooth	< 0.19 cm
Intermediate	0.19 → 1.06 cm
Rough	> 1.06 cm

h = 12.0 cm – Rough, bright

h = 1.0 cm -- Intermediate

h = 0.2 cm ~smooth, dark

Roughness at Copper Canyon

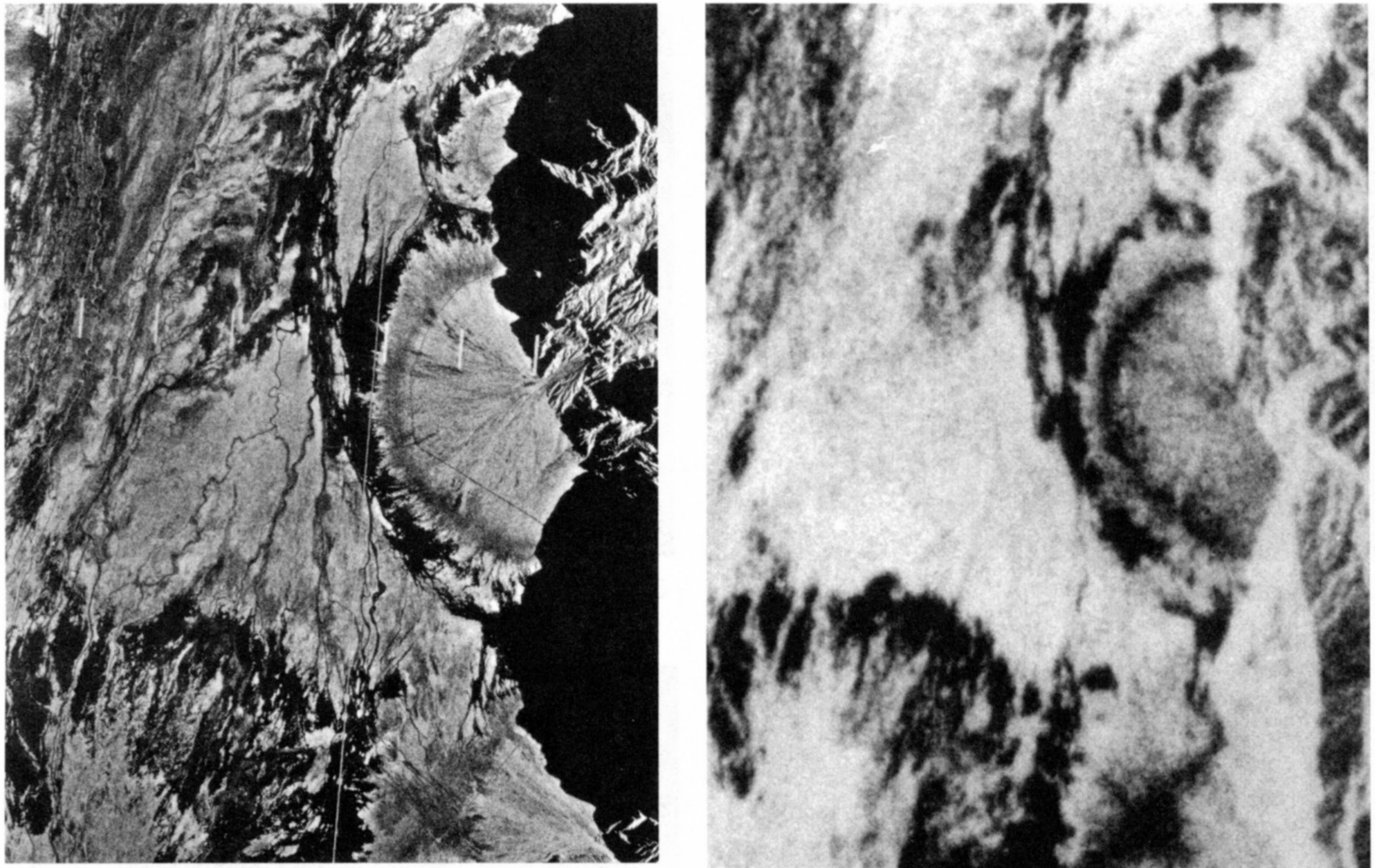

A. X-band image (3.0-cm wavelength).

B. L-band image (23.5-cm wavelength).

Sabins Fig. 6-36
(pg. 206)

Main difference may be lower resolution of L band data

(λ is 8 $\times$ larger, so R_a 8 $\times$ worse if all else is equal)

Also have some effect from different "roughness" limits

	X (3.0 cm)	L (23.5 cm)
Smooth	< 0.19 cm	< 1.46 cm
Rough	> 1.06 cm	>8.31 cm

Roughness at Copper Canyon

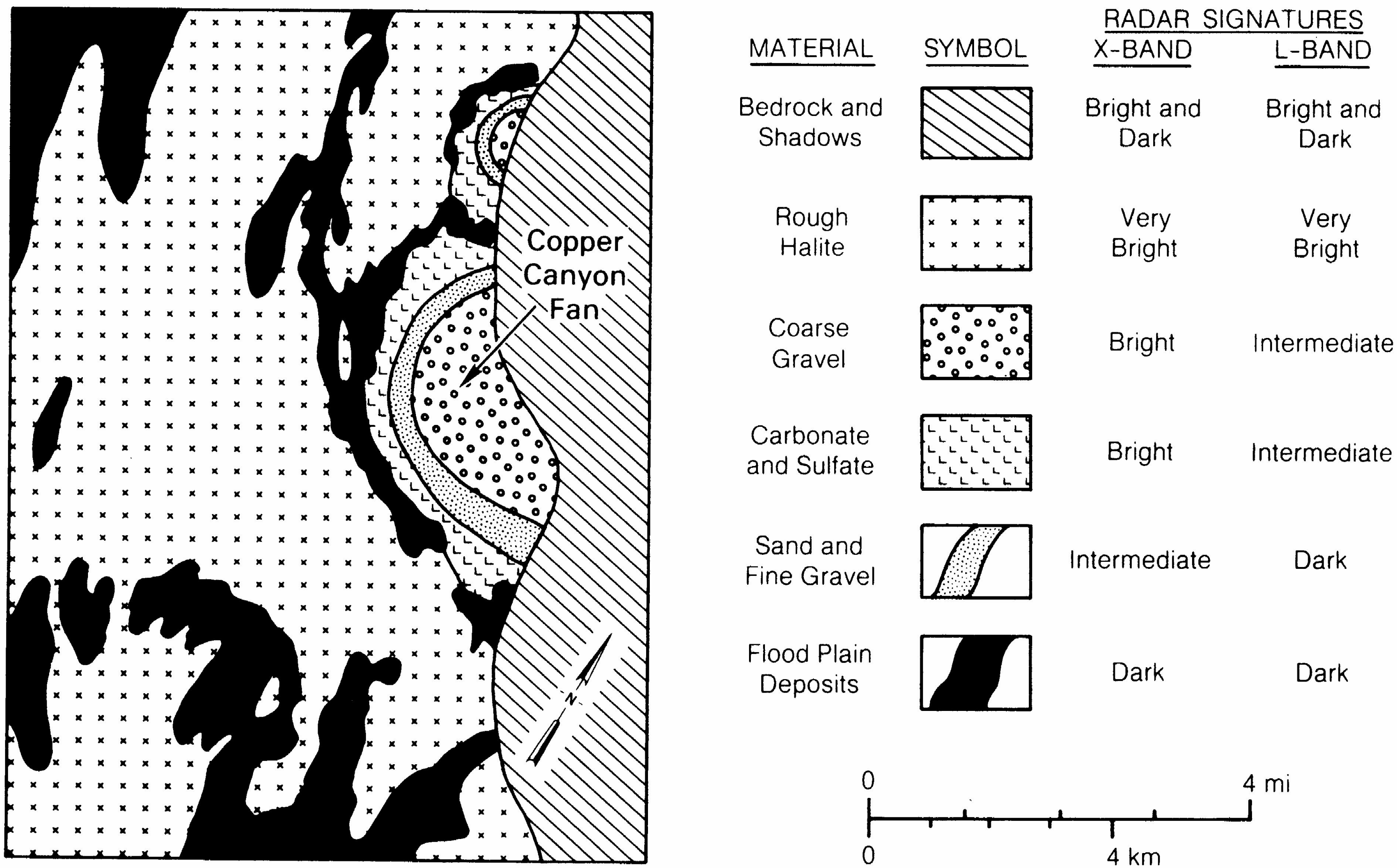

C. Interpretation map.

D. Map explanation.

Figure 6-36 X-band and L-band images of the Copper Canyon alluvial fan and vicinity, Death Valley. From Sabins (1984, Figures 9, 10).

Sabins Fig. 6-36
(pg. 206)

Dielectric Constant

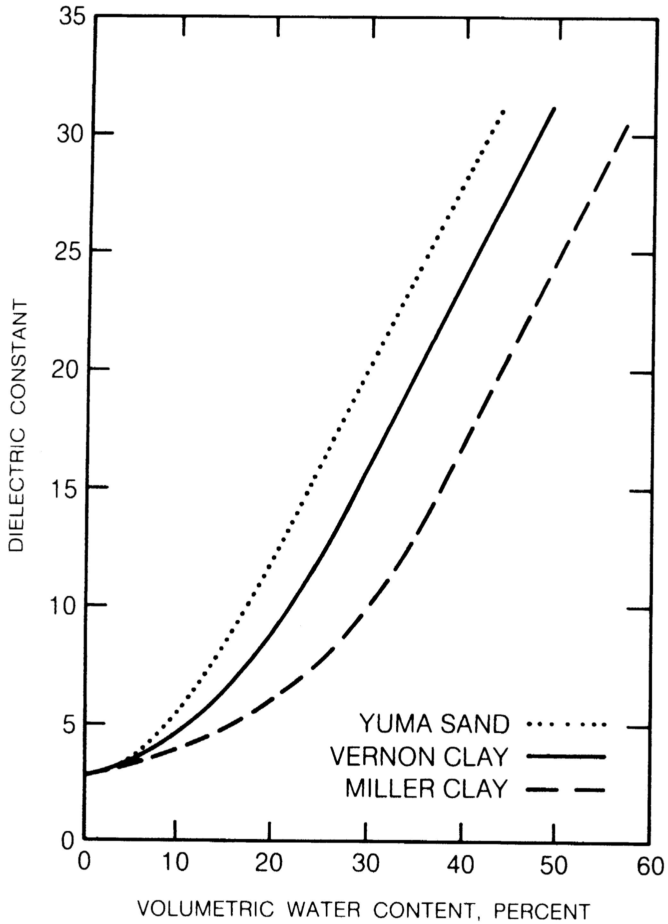

Figure 6-27 Variation of dielectric constant (at 27-cm wavelength) as a function of moisture content in sand and clay. From Wang and Schmugge (1980, Figure 3).

Sabins Fig. 6-27

Dielectric Constant:
  Amount of “polarizability” of medium
  reduces internal E field

Index of refraction $n \propto \varepsilon^{1/2}$

At radio (radar) frequencies
the polar H_2O molecules can partially align,
giving large ε:

Rock and dry soil: $\varepsilon \sim$ 4 to 8

Water: $\varepsilon \sim 80$

So a small amount of water changes
index of refraction (and scattering) a lot.

Moisture and Scattering

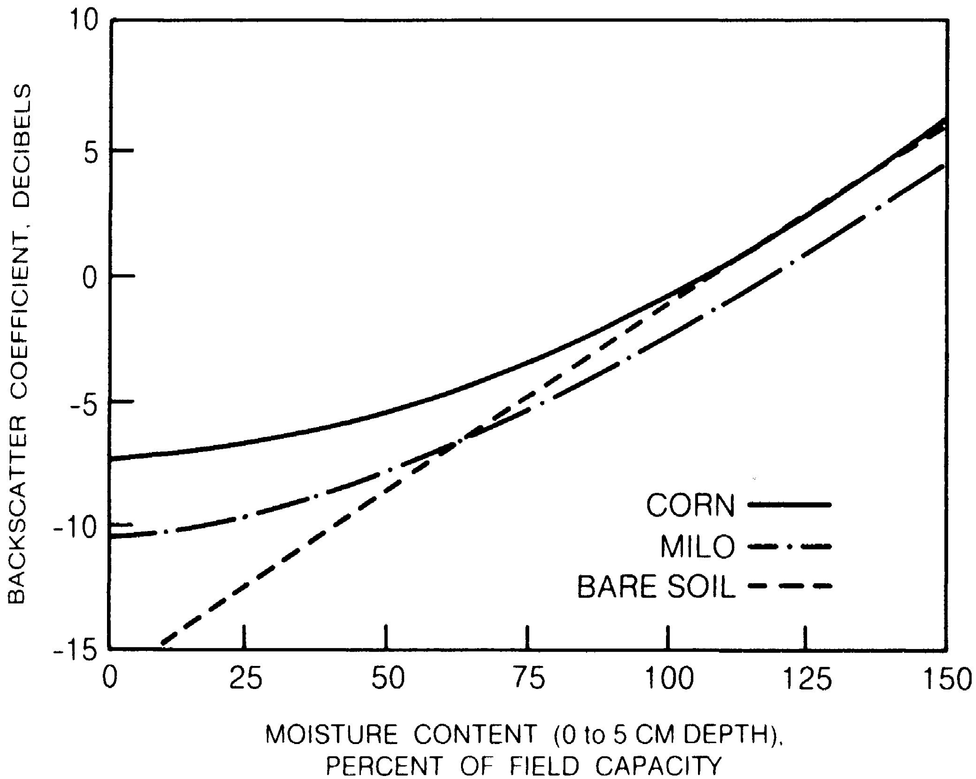

Figure 6-28 Variation of backscatter (at 6.7-cm wavelength) as a function of moisture content. Milo is a grain resembling millet. From Ulaby, Aslam, and Dobson (1982, Figures 4 and 7).

Using
Backscatter Coefficient σ
to estimate
soil moisture content

Sabins Fig. 6-28

Radar after rainstorm

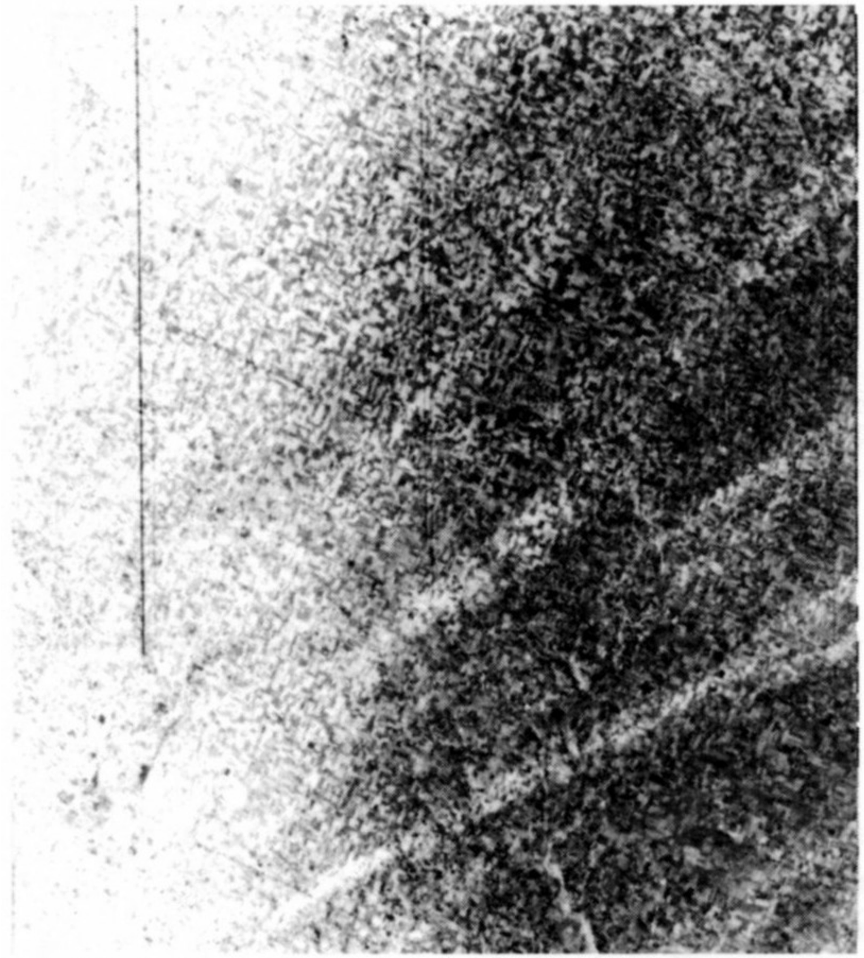

A. Radar image.

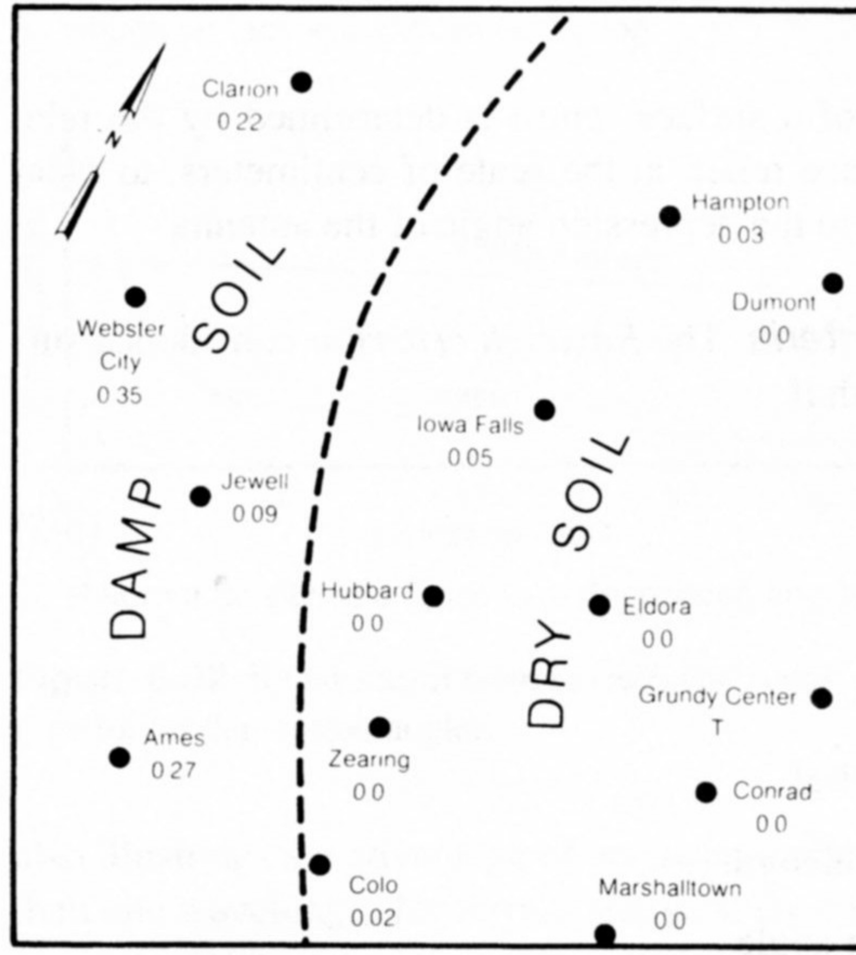

B. Map showing rain-gauge data.

Sabins Fig. 6-29, from Ulaby et al, 1983

Damp soil is much more reflective